OBJECTIVE: Tsunami Society International publishes this journal to increase and disseminate knowledge about tsunamis and their hazards.

DISCLAIMER: Although the articles in SCIENCE OF TSUNAMI HAZARDS have been technically reviewed by peers, Tsunami Society International is not responsible for the veracity of any statement, opinion or consequences.

Submit manuscripts of articles, notes or letters to the Editor. If an article is accepted for publication the author(s) must submit a scan-ready manuscript, a Doc, TeX or a PDF file in the journal format. Issues of the journal are published electronically in PDF format. Issues of the journal (ISSN 8755-6839) from 1982 thru 2005 are available in PDF format at http://epubs.lanl.gov/tsunami/and at **WWW.TSUNAMISOCIETY.ORG** or on a CD-ROM that may be purchased by contacting Tsunami Society International at tsunamisociety@hawaiiantel.net Recent and all past journal issues are also available at: http://www.TsunamiSociety.org

Tsunami Society International members are notified by e-mail when a new issue is available. There are minimal page charges for authors who are members of Tsunami Society International for three years and slightly higher for non-members. Permission to use figures, tables and brief excerpts from this journal in scientific and educational works is hereby granted provided that the source is acknowledged.
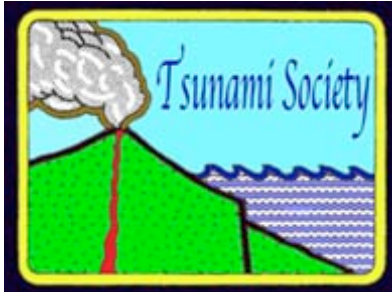
THE RESPONSE OF MONTEREY BAY TO THE 2010 CHILEAN EARTHQUAKE

Laurence C. Breaker[1], T. S. Murty[2] , Stephanie J. Flora[1] and Craig N. Hunter[1]

[1] Moss Landing Marine Laboratories, Moss Landing, CA 95039
[2] University of Ottawa, Ottawa, Canada

ABSTRACT

The primary frequencies contained in the arrival sequence produced by the tsunami from the Chilean earthquake of 2010 in Monterey Bay were extracted to determine the seiche modes that were produced. Singular Spectrum Analysis (SSA) and Ensemble Empirical Mode Decomposition (EEMD) were employed to extract the primary frequencies of interest. The wave train from the Chilean tsunami lasted for at least four days due to multipath arrivals that may not have included reflections from outside the bay but most likely did include secondary undulations, and energy trapping in the form of edge waves, inside the bay.

The SSA decomposition resolved oscillations with periods of 52-57, 34-35, 26-27, and 21-22 minutes, all frequencies that have been predicted and/or observed in previous studies. The EEMD decomposition detected oscillations with periods of 50-55 and 21-22 minutes. Periods in the range of 50-57 minutes varied due to measurement uncertainties but almost certainly correspond to the first longitudinal mode of oscillation for Monterey Bay, periods of 34-35 minutes correspond to the first transverse mode of oscillation that assumes a nodal line across the entrance of the bay, a period of 26-27 minutes, although previously observed, may not represent a fundamental oscillation, and a period of 21-22 minutes has been predicted and observed previously. A period of ~37 minutes, close to the period of 34-35 minutes, was generated by the Great Alaskan Earthquake of 1964 in Monterey Bay and most likely represents the same mode of oscillation. The tsunamis associated with the Great Alaskan Earthquake and the Chilean Earthquake both entered Monterey Bay but initially arrived outside the bay from opposite directions. Unlike the Great Alaskan Earthquake, however, which excited only one resonant mode inside the bay, the Chilean Earthquake excited several modes suggesting that the asymmetric shape of the entrance to Monterey Bay was an important factor and that the directions of the incoming tsunami-generated waves were most likely different.

Science of Tsunami Hazards, Vol. 30, No. 1, page 1 (2011)

The results from SSA and EEMD produced results that differed. Although a period of 34-35 minutes was observed in the SSA, it was not detected in the EEMD. In previous comparisons, however, we have observed that oscillations detected in EEMD were not detected in SSA. SSA also revealed an oscillation with a period of 26-27 minutes, not observed in the EEMD. This oscillation, however, may not represent a fundamental mode but instead a harmonic related to the first longitudinal mode of oscillation whose period is ~55 minutes. We conclude that both methods were useful in helping to interpret the results of this study.

Keywords: Monterey Bay, 2010 Chile Earthquake, Bay Response, Great Alaska Earthquake, spectral decomposition

1. INTRODUCTION

When tsunamis from the open ocean enter coastal waters and embayments they often excite secondary oscillations whose periods are primarily determined by the boundaries that constrain them. Such oscillations are often referred to as free or natural oscillations or seiches. The natural oscillations of Monterey Bay have been a subject of study since the mid-1960s. The seiche modes of Monterey Bay were first examined by Wilson, Hendrickson, and Kilmer (WHK; 1965). They applied both analytical and numerical techniques using various simple geometrical shapes to approximate the bay in order to extract its natural modes of oscillation. In applying these methods, a nodal line was assumed to exist across the mouth of the bay from the Monterey Peninsula to Santa Cruz (Fig.1).
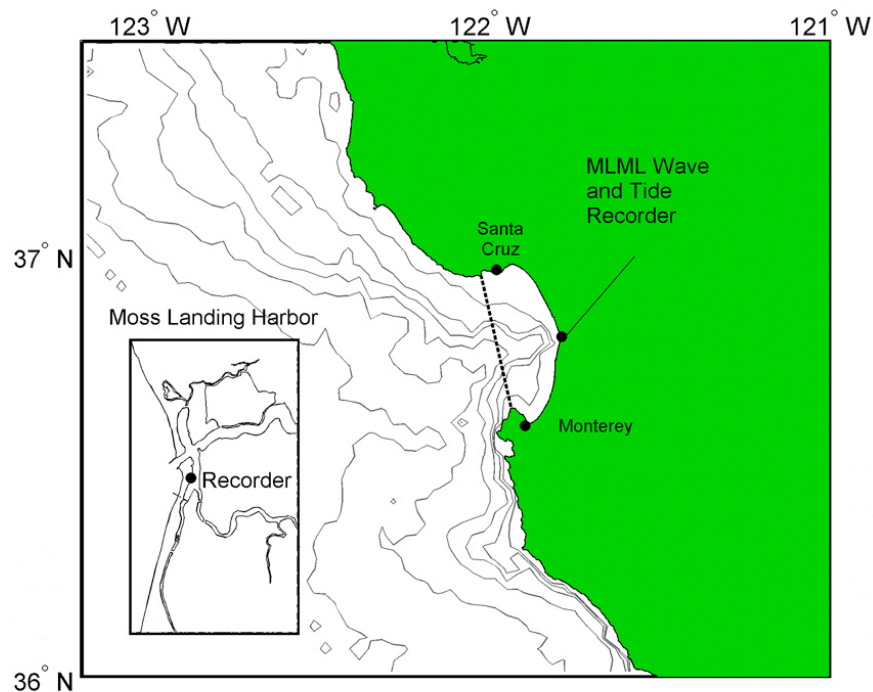

Figure 1. Map of the study area with an inset showing the location of the tide gauge in Moss Landing Harbor. The depth contours starting at the coast are 50, 100, 200, 500, 1000, and 2000 meters.

In describing the oscillating characteristics of the bay as a whole, we refer to the mode of oscillation oriented in the North-South direction as longitudinal, and the mode of oscillation oriented in the East-West direction as transverse. In addition to longitudinal and transverse modes of oscillation, WHK indicated that many higher modes of oscillation can be excited that are primarily restricted to certain parts of the bay including Monterey Harbor. Based on model results, they also found that the Monterey Submarine Canyon (MSC) separates the bay into two semi-independent halves with only weak coupling between them. Finally, periods were predicted for the lowest modes of oscillation in Monterey Bay with values of 44.2, 29.6, 28.2, 23.3, 21.6, and 20.4 minutes for the first 6 modes.

Subsequent studies have consistently shown natural periods of oscillation for the bay of approximately 55, 36, 27, and 21 minutes (e.g., Lynch, 1970; Breaker et al., 2008; Breaker et al., 2010), where an oscillation with a period of 55 minutes corresponds to the first longitudinal mode, and an oscillation with a period of 36 minutes corresponds to the first transverse mode. The response of Monterey Bay to the Loma Prieta Earthquake of 1989 and the Great Alaskan Earthquake of 1964 were recently examined by Breaker et al. (2009). They found that it is not clear how or where the tsunami associated with the Loma Prieta Earthquake was generated, but it occurred inside the bay and most likely began to take on the characteristics of a seiche by the time it reached the tide gauge in Monterey Harbor. Two primary periods of oscillation were found, one with a period 9-10 minutes, and the second with a period of 31-32 minutes. The first oscillation is in agreement with the range of periods for the expected natural oscillations of Monterey Harbor, and the second oscillation is consistent with a bay-wide oscillation or seiche mode. For the Great Alaskan Earthquake, which entered the bay across its mouth, several sequences of oscillations, all with a period of approximately 37 minutes, were found which corresponds to the transverse mode of oscillation. Finally, the sea level responses to these events differed greatly because different modes of oscillation were excited in each case.

Breaker et al. (2010) employed tidal data and numerical simulations to examine the oscillating characteristics of the bay. The model results were consistent with earlier studies, suggesting that the MSC separates the bay into two oscillating basins. However, water level and pressure data examined during the study indicated that oscillations corresponding to the four lowest natural frequencies (with periods of 55, 36, 27, and 21 minutes, respectively) tended to be bay-wide. Spatial patterns extracted from model-generated power spectra at the four lowest frequencies agreed closely with the modal patterns predicted by WHK. It was found that in addition to transient responses due to winter storm activity, low amplitude seiche oscillations occur on a continuous basis at the four lowest frequencies. Model simulations further indicated that both the winds and tides contribute to the oscillations.

The Chilean earthquake of 2010 occurred on February 27th at 06:34 UTC and lasted for approximately 90 seconds. The epicenter was located at 35.91°S, 72.73°W off the coast of central Chile at a depth of 35 km. The intensity of this event was 8.8 on the moment magnitude scale. This earthquake triggered a tsunami that spread across the Pacific basin. This event caused damage along the California coast at least as far north as San Diego. According to the Pacific Tsunami Warning Center, the observed maximum height of the tsunami at Monterey, California was 0.28 m with an arrival time of 20:31 UTC, almost 14 hours after the initial shock. An earthquake of magnitude 6.9 occurred approximately 90 minutes after the main event whose epicenter was located about 300km southwest of the location of the initial earthquake but may have not been related to it (U.S. Geological Survey, 2010).

In the present study, we examine water levels recorded during the Chilean earthquake of 2010 inside Monterey Bay to determine how the bay responded to this event. In the process, we compare the bay's response in this case with the bay's response to the Great Alaskan Earthquake of 1964. Our primary goal is to extract the frequency content of the tsunami-generated signals to determine what modes of oscillation were excited in Monterey Bay as a result of the Chilean earthquake of 2010. To accomplish this goal, we employ two methods of spectral decomposition, Singular Spectrum Analysis (SSA) and Ensemble Empirical Mode Decomposition (EEMD).

2. DATA ACQUISITION AND ANALYSIS

a. Data Acquisition

The water level data employed in this study were acquired in Moss Landing Harbor. Moss Landing is located almost equidistant from the north and south ends of Monterey Bay (Fig. 1). The instrument used to record the water level data is a SEA-BIRD Electronics SBE 26 Seagauge wave and tide recorder. The recorder is located next to the dock at the Moss Landing Small Boats Facility in Moss Landing Harbor (36.807°N, 121.788°W). The gauge is suspended from a piling one meter above the bottom. The measured water levels are thus directly proportional to the height of the water column directly above the gauge. The sampling interval is five minutes (0.0833 hours). As a result, the uncertainty in resolving the periods of interest (or any other period) is $\pm$ 2.5 minutes. The original record for the period from February 27 through March 6, 2010 is shown in Fig. 2.
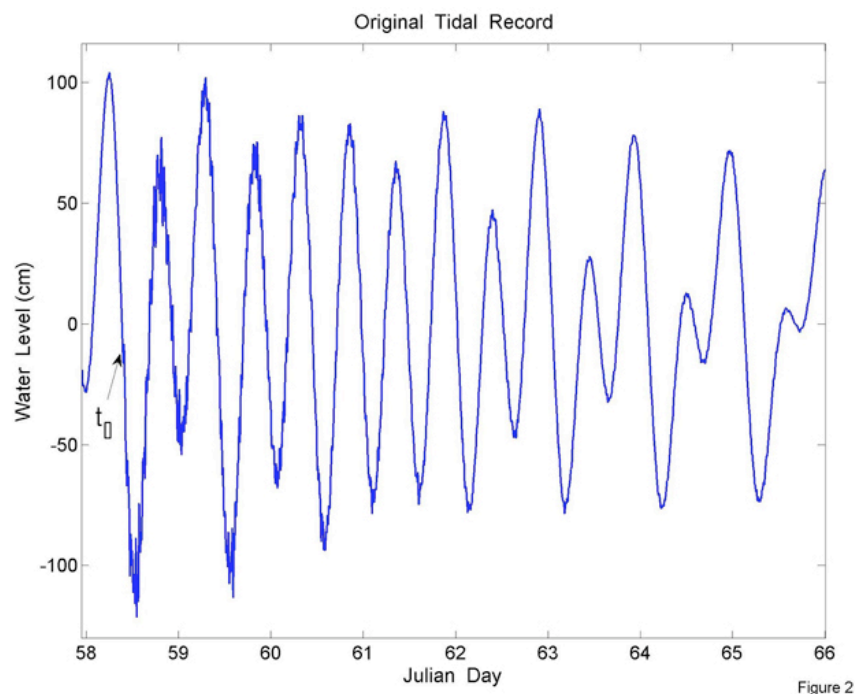

Figure 2. The original water level record acquired during the period of the Chilean earthquake of 2010 from the tide gauge in Moss Landing Harbor.

The first arrival is indicated by t_0 and, as stated above, occurs on Julian Day 58 at 06:34 UTC. Because the amplitude of this event is relatively small compared to the amplitude of the diurnal and semidiurnal tides in Monterey Bay it is difficult to observe in the original data. However, by using SSA and EEMD we were able to isolate and examine this event in detail.

b. Methods of Analysis

A primary objective of this study is to extract the frequency content of the tsunami-generated signals that were recorded in order to determine what modes of oscillation were excited in Monterey Bay from the Chilean earthquake of 2010. To determine the frequency content of these signals we have employed Singular Spectrum Analysis (SSA) and Ensemble Empirical Mode Decomposition (EEMD). Both methods decompose the data into a sequence of quasi-independent modes and are well suited for analyzing short, noisy records. In using SSA, the number of modes that the data are decomposed into is determined by the user whereas in EEMD, the number of modes is determined by the data. To illustrate the basic differences in how these methods are formulated, brief introductions to SSA and EEMD are given in Appendices A and B along with details concerning their implementation in this study.

3. RESULTS

a. Results from SSA

The Chilean earthquake of 2010 occurred on February 27th at 0634UTC. The recording at Moss Landing showed that this event lasted for at least four days before the amplitudes of all tsunami-related arrivals had decreased to background levels. In applying SSA to this record a window length (L) of 600 (600 x 0.08333 = 50 hours) was initially used. The eigenvalues are shown in the upper panel of Fig. 3. They represent the variance associated with each mode and, by convention, are plotted in descending order. The eigenvalues are plotted on a logarithmic scale in deciBels (dB). The first two eigenvalues form a pair that represents a single oscillation where the corresponding eigenvectors and principal components are in quadrature. The same is true for the 3rd and 4th eigenvalues. The first pair corresponds to the semidiurnal tide and the second to the diurnal tide. In order to examine the modes of interest in greater detail we have subtracted the reconstructed components for the first four modes to remove the influence of the tides and then subjected the residuals to SSA, in this case using a window length of 12 (12 x 0.08333 = 1 hour). Following the terminology of Golyandina et al. (2001), we refer to the results of this decomposition as Sequential SSA. The results are shown in the lower panel of Fig. 3.

Next, we examine the reconstructed components (RCs) from the Sequential SSA (Fig. 4). The vertical axes are expressed in cm and the x-axis extends from Julian Day 58 (February 27, 2010 to Julian Day 66 (March 7, 2010). First, we have summed RCs 1-4 to compare the maximum amplitude of the tsunami arrivals with that reported by the Pacific Tsunami Warning Center (PTWC). We obtain a maximum amplitude of approximately 20 cm compared to 28 cm reported by the PTWC. Our value

is somewhat lower and could be due in part to the fact that the value reported by the PTWC was obtained from the tide gauge in Monterey Harbor located almost 20 km SSW of Moss Landing.
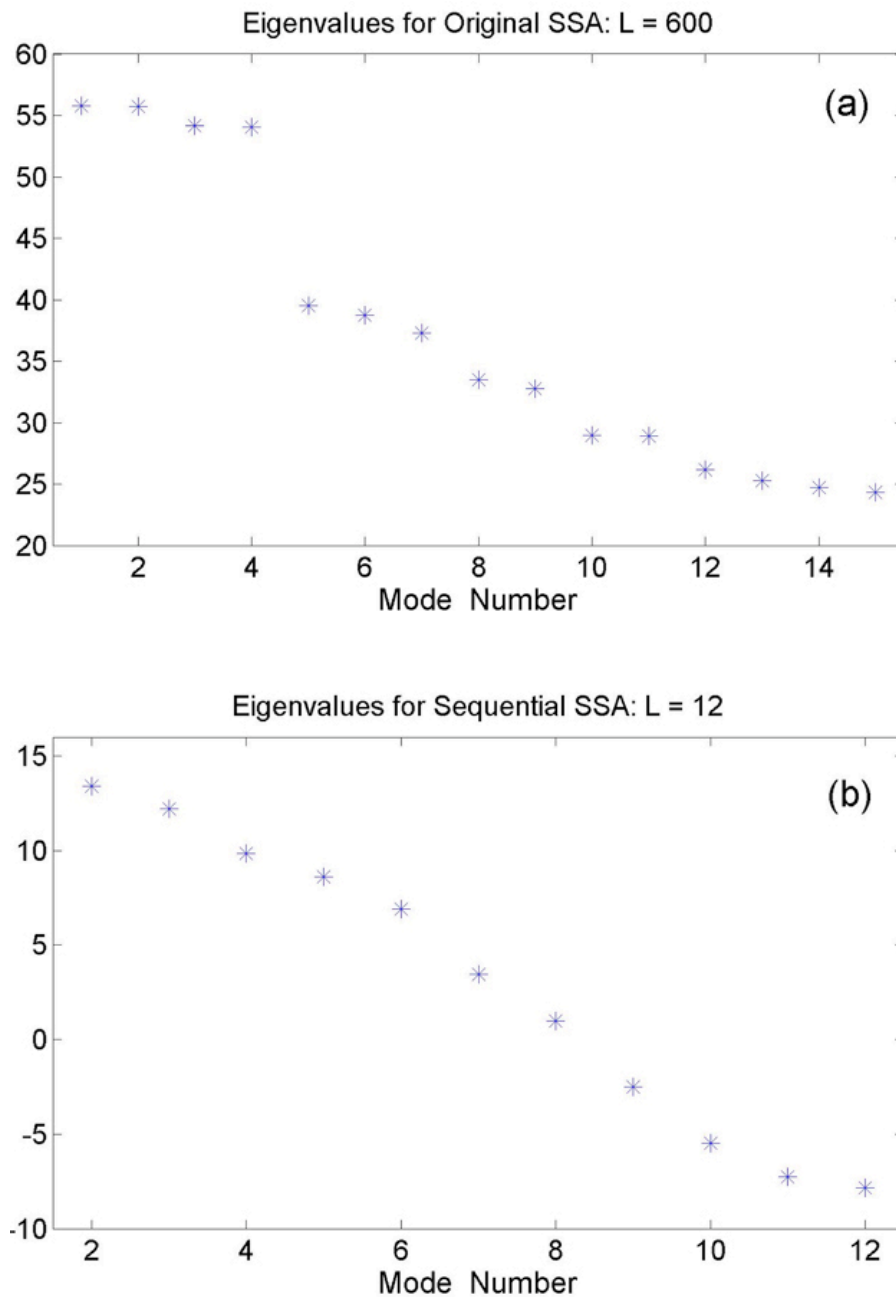
Figure 3. Eigenvalues from Singular Spectrum Analysis (SSA) for the original decomposition using a window length of 600 (50 hours) in the upper panel (a), and the eigenvalues from SSA after removing the first four reconstructed components from the original decomposition in the lower panel (b). The vertical axis is plotted on a logarithmic scale in deciBels (dB).
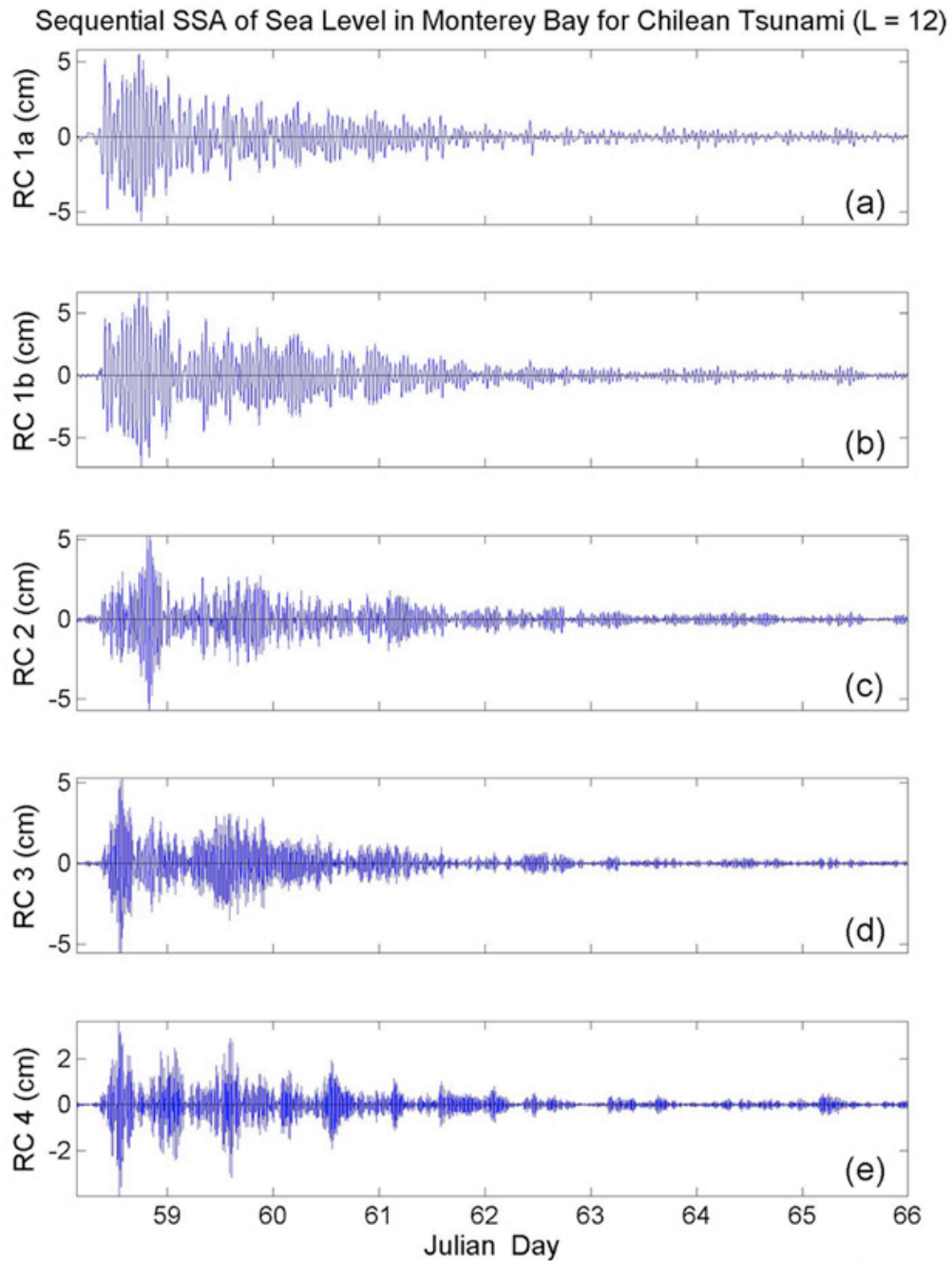
Figure 4. Reconstructed components (RCs) from the sequential SSA using a window length of 12 for Julian Days 58 through 65 showing an oscillation with periods of ~55 minutes (RCs 1a and 1b) in the top two panels (a & b), RC from the sequential SSA showing an oscillation with a period of 34-35 minutes (RC 2) in the third panel (c), RC from the sequential SSA showing an oscillation with a period of 26-27 minutes (RC 3) in the fourth panel (d), RC from the sequential SSA showing an oscillation with a period of 21-22 minutes (RC 4) in the fifth panel (e).

Continuing, we now examine the RCs or partial time series for frequency content. We found that the periods varied somewhat according to the number of modes that the data were originally decomposed into, and according to where in the arrival sequence we measured the periods. The first observation comes as no surprise since we expect that as *L* is increased, the effective bandwidth of each mode is decreased and so the variation in frequency is constrained to become smaller. After some experimentation we settled on a window length of 12 (1 hour) and have used this value throughout the analysis. Perhaps the most compelling reason for choosing this window length, however, is that it matches the number of Intrinsic Mode Function components (IMFs) that were obtained in the subsequent EEMD decomposition where the number of IMFs is determined by the data and so is not a free parameter chosen by the user. The second issue was more problematic but if any systematic patterns in the periods over an arrival sequence could be found it was that they tended to decrease slightly further into the sequence. What we report, however, are mean values estimated from samples taken at different locations throughout the sequence over the first 4 days. To summarize, RCs 1a and 1b produced a period with a mean value that falls between 52 and 57 minutes. In this case, there was a rather clear trend toward slightly shorter periods, as measurements were made further into the arrival sequence. We note that a period of approximately 55 minutes corresponds closely to the expected period for the first longitudinal mode of oscillation in Monterey Bay. The second RC has a period of 34-35 minutes and is close to the expected period for the first transverse mode of oscillation for Monterey Bay (~36 minutes). The third RC has a mean period of 26-27 minutes and has previously been observed on several occasions (e.g., Lynch, 1970). The fourth RC has a mean value of 21-22 minutes and is in close agreement with the value predicted by WHK (21.6 minutes) and observed in other studies (e.g., Breaker et al., 2008; Breaker et al., 2010). The results from the SSA decomposition are summarized in Table 1 below.

Returning to Fig. 3, the eigenvalues for the first two modes represent a single (well-defined) oscillation since the corresponding eigenvectors and principal components are in quadrature (not shown). However, the next three modes do not represent pure oscillations since they each correspond to a different frequency (Fig. 4). The explanation for this is that in the first case for oscillations with a period of approximately 55 minutes, there are approximately 11 samples per cycle for a sampling interval of 5 minutes, producing a waveform that closely approximates a pure sinusoid. However, for the next three modes with periods of 34-35, 26-27, and 21-22 minutes, the number of samples per cycle decreases yielding waveforms that increasingly depart from a pure sinusoid. For a period of 21-22 minutes, for example, there are only about 4 samples per cycle yielding a waveform that is far from sinusoidal and much closer to a saw tooth pattern. Thus, the decomposition treats the shorter undersampled periods as separate frequencies rather than oscillatory pairs.[1]

---

[1] Undersampling also made it more difficult to estimate the true periods of the oscillations in these cases.

Table 1. Period extraction using Singular Spectrum Analysis and Ensemble Empirical Mode Decomposition

Modal Sequence[1]	Singular Spectrum Analysis (SSA)	Ensemble Empirical Mode Decomposition (EEMD)	Comments
1	21 – 22 minutes	21 – 22 minutes	Previously predicted and observed
2	26 – 27	-------	May be 1st harmonic of 4th mode
3	34 – 35	-------	Close to observed transverse mode
4	57 –> 52[2]	55 –> 50[2]	Previously predicted and observed

[1] From shortest to longest periods.
[2] "–>" indicates that the period gets shorter further into the arrival sequence.

b. Results from EEMD

The results from the EEMD decomposition are shown in Fig. 5. The data are decomposed into 12 IMFs. Following Huang et al. (1998), the IMFs are ordered by frequency in descending order. The last IMF, IMF 12, in this case, is usually referred to as the residual and often corresponds to a long-term trend, if one exists. IMFs 3, 4, 5 and 6 contain the semidiurnal (IMFs 3 and 4) and diurnal (IMFs 5 and 6) tides. The higher modes are not of interest to us and so will not be discussed. Of primary interest are IMFs 1 and 2, which contain the tsunami-related signals. The separation between IMFs 2 and 3 is not complete as shown by the slight degree of mode mixing in IMF 3 during Julian Days 58 and 59. Although this reduces the variance in IMF 2, its impact is small and does affect the interpretation of our results. [2]

Analogous to the manner in which the eigenvalues are plotted by mode number in Fig. 3, we have plotted the variances for each IMF from EEMD in Fig. 6. The variances associated with the tsunami arrivals for IMFs 1 and 2 are small compared to the variances for the modes associated with the primary tidal constituents (IMFs 3, 4, and 5, and to a lesser extent, IMF 6), consistent with our interpretation of the eigenvalues shown in Fig. 3. The first two IMF components are plotted separately in Fig. 7 with the amplitudes expressed in cm. When IMF1 and IMF2 are combined, we obtain a peak amplitude of 22cm, close to the value obtained by summing the relevant RCs from SSA (20cm). The frequency analysis of IMF1 yields periods in the range of 21-22 minutes, virtually identical to the results we obtained from SSA. The second IMF (IMF2) yields periods in the range of 50-55 minutes,

---

[2] To ensure a level playing field in comparing SSA and EEMD, we also conducted EEMD using the residuals obtained from Sequential SSA and obtained almost the same results. However, there was slightly greater mode mixing between modes 2 and 3 and so we have not used the residuals from the SSA as the starting point for conducting EEMD.

similar, but not identical to the results we obtained for RC 4 from SSA. Again, there was a tendency for the periods to decrease slightly as measurements were made further into the arrival sequence between Julian Days 58 and 62. What we find particularly noteworthy are the absences of oscillations with periods of 26-27 minutes and 34-35 minutes, oscillations that were extracted using SSA. The results from the EEMD decomposition are summarized in Table 1.
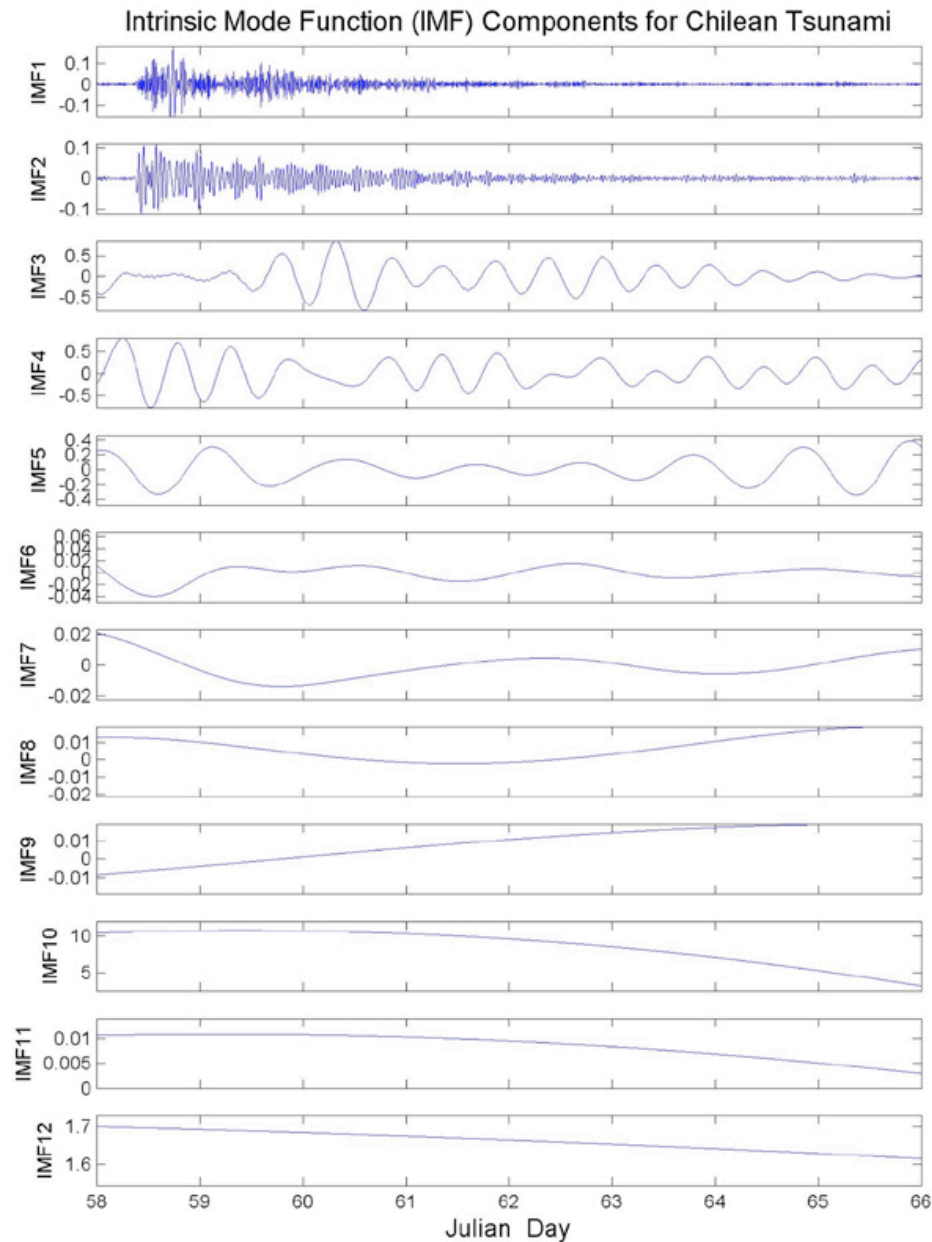
Figure 5

Figure 5. Intrinsic Mode Function Components (IMFs) from the EEMD decomposition. The first two IMFs (IMF1 and IMF2) show the wave trains for separate contributions from the Chilean earthquake.
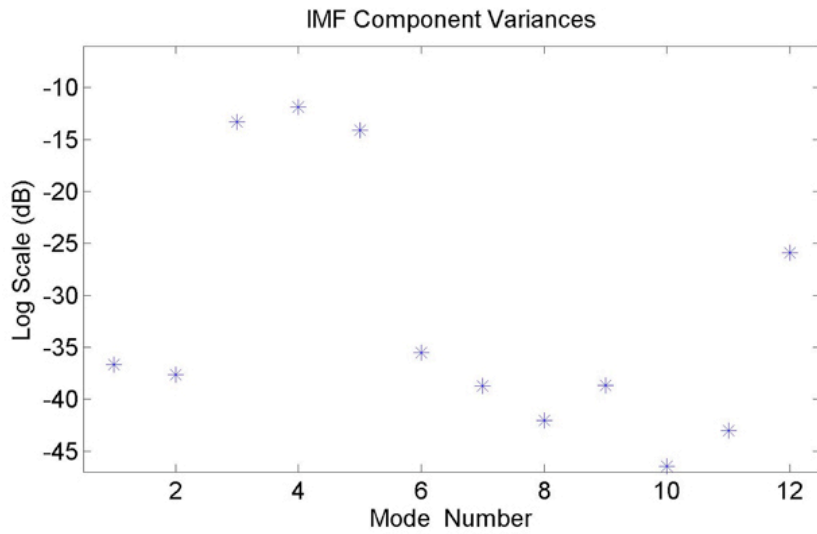
Figure 6. The variances are shown for each IMF component and are plotted in dB. The first two IMFs correspond to the variances associated with the first two IMF components shown in Fig. 5.
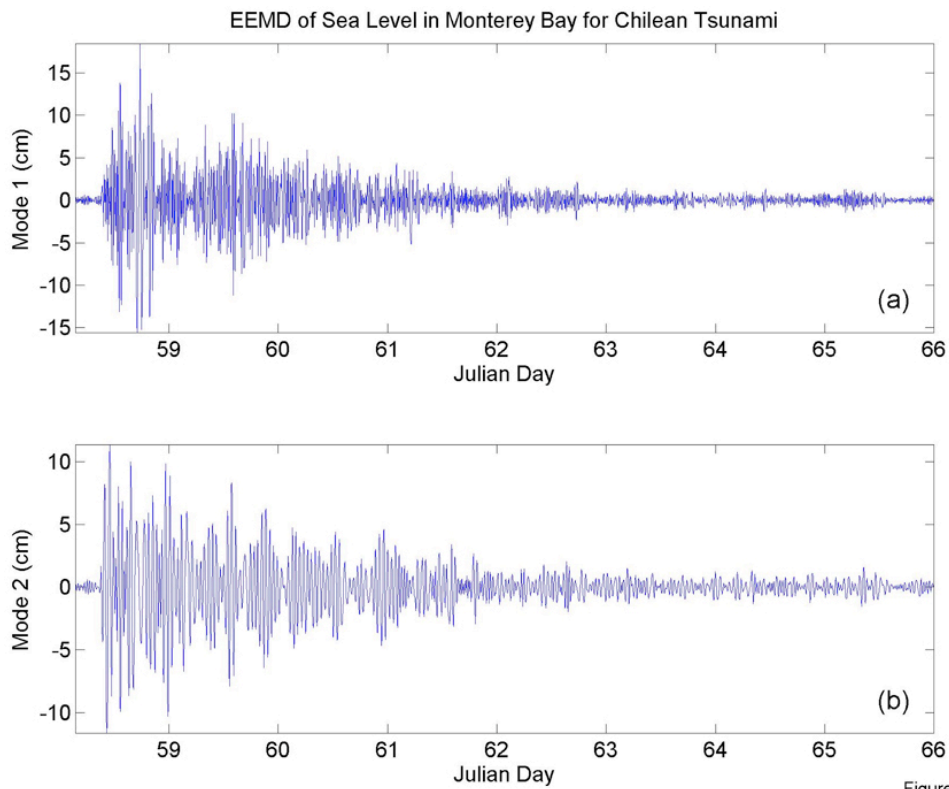
Figure 7. The first two IMF Components from the EEMD decomposition. The top panel (a) shows IMF1 with a primary period in the range of 21-22 minutes, and the bottom panel (b) shows IMF2 with a primary period in the range of 50-55 minutes.

c. Interpretation of the results

First we point out that the 6.9 magnitude earthquake that followed the main event by approximately 90 minutes may have contributed to the arrival sequence within the first few cycles since earthquakes with magnitudes that exceed 6.4 often produce tsunamis (Wilson, 1962). However, its impact must be considered small since it was far weaker than the main event.

The modal patterns for the frequencies associated with the natural oscillations of Monterey Bay were first predicted by WHK and more recently predicted and compared with observations by Breaker et al. (2010). RCs 1a and 1b from SSA and IMF2 from EEMD revealed periods in the range of 50-57 minutes consistent with the first longitudinal mode of oscillation for Monterey Bay. Model results from WHK and Breaker et al. (2010) suggest that MSC acts to separate the bay into two oscillating basins but water level data from Monterey and Santa Cruz (Fig. 1) indicate that the oscillations with the longest periods (55, 36, 27 and 21 minutes) span the entire bay. However, at higher frequencies, Breaker et al. (2010) concluded that MSC might serve as a more effective barrier. According to past observations, oscillations with periods of approximately 36 minutes correspond to the first transverse mode with a nodal line that is assumed to extend across the entrance of Monterey Bay (Fig. 1; Lynch, 1970; Breaker et al., 2008; Breaker et al., 2010). The results from SSA in response to the Chilean earthquake of 2010 reveal an oscillation with a period of 34-35 minutes, very close to this value. Breaker et al. (2009) in their examination of Monterey Bay's response to the Great Alaskan Earthquake of 1964 found that the resulting oscillations all had a period of approximately 37 minutes, consistent with an ocean wave that enters the bay across the entrance. As the wave enters Monterey Bay it conforms to the bay's dimensions and in the process is transformed into a seiche with a period that has been approximately predicted and closely observed on previous occasions. It was also noted that an oscillation with a node across the mouth of the bay and an antinode near Moss Landing is clearly reminiscent of quarter wave resonance. RC 3 from the SSA revealed a period 26-27 minutes. Observations with periods in this range have been previously reported but the true source of this oscillation is open to question. We discuss this issue in greater detail in section 4. Finally, SSA revealed a period of 21-22 minutes, which has been predicted by WHK and observed on numerous occasions. Its predicted spatial pattern spans the entire bay with antinodes at each end and a third antinode located at the center of the bay near Moss Landing.

As indicated earlier, IMF1 from EEMD revealed periods in the range of 21-22 minutes consistent with our results from SSA. IMF2 revealed periods in the range of 50-55 minutes, generally consistent with our results from SSA (52-57 minutes). In both cases, the periods tended to become shorter further into the arrival sequence, creating a signal that is slightly frequency modulated. Whether or not these variations simply reflect measurement uncertainties or are real is not clear, but emphasize the difficulties that arise in trying to estimate these periods.

Returning to Figs. 4 and 7, oscillatory behavior can be detected in the tsunami-generated signals for at least four days following the first arrival on Julian Day 58. As stated in Camfield (1980), the actual form of the wave train is initially determined by the generating mechanism, which includes the area of the uplifted sea bottom, the height and variation of the uplifted area, the depth of water, and related characteristics of the generating area. Between the epicenter and the observing site, multipath effects also spread the arrival pattern over time. As we examine each figure we see that the wave trains consist of arrival packets or groupings where the signal amplitudes are higher for periods

of several hours or longer and often repeat out to Julian Days 62 or 63 where the amplitudes finally decay to background levels. These extended or secondary oscillations may include reflections from outside or inside the bay, secondary undulations and/or energy trapping.   Because the epicenter was located near the coast of Chile there are no obvious major reflecting boundaries between the epicenter and Monterey Bay in the eastern Pacific that would appear to contribute to the observed arrival sequence. If we are correct, then the observed arrival patterns are primarily due to processes that occur inside the bay. The arrival patterns in Figs. 4 and 7 in most cases display at least some degree of amplitude modulation. In Figs. 4e (RC 4) and 7b (IMF 2) the modulation patterns tend to be cyclic with periods of roughly 14 and 9 hours, respectively, indicating constructive reinforcement at preferred times.

Next we consider the importance of secondary undulations. Secondary undulations are oscillations whose periods correspond to the normal modes of a particular embayment that can be excited by several mechanisms including tsunamis (Kowalik and Murty, 1993). In most cases, they can be classified as one of three types, A, B, or C, depending on the geometry of the bay (Nakano, 1932). In type A, the secondary undulations appear as coherent wave trains with approximately the same waveform. In type B, they are not as regular and coherent as in type A, but are not completely irregular. In type C, the arrival patterns are essentially irregular. The type of secondary undulations can be roughly determined by plotting the depth of the bay versus $10S/b^2$, where S corresponds to the surface area of the bay, and b, its width. Monterey Bay has a length of approximately 40 km and a width of approximately 20 km and so has a surface area, S, of roughly 800 km^2. With an average depth of 100m, the secondary undulations fall into category B, where they are not as regular and coherent as in type A, but are not completely irregular. This result is generally consistent with the oscillatory patterns exhibited, but is, to some degree, mode dependent. This result is also consistent with a similar analysis performed by Breaker et al. (2009) for Monterey Bay who found that the wave trains associated with the Loma Prieta earthquake of 1989 and the Great Alaskan Earthquake of 1964 produced patterns consistent with type B.

Finally, we consider energy trapping as a third process that may contribute significantly to the observed arrival sequences. Energy trapping can take place along continental shelves and details concerning the types of wave motion that can be supported under such conditions are given in Murty et al. (2005) and Murty et al. (2008). Edge waves are one of several types of waves that can occur along continental shelves. Seiches have been known to produce edge waves in several cases (e.g., Murty et al., 2006). In certain situations, the energy associated with a given seiche mode can excite edge waves with the same period. Edge waves occur in the infragravity wave frequency band and significant energy has been observed in the shallow reaches of Monterey Bay in this range (MacMahan et al., 2004a; MacMahan et al., 2004b).

The following relationship given by Yanuma and Tsuji (1998) predicts the period, T, of a standing edge wave

$$T(M,L,a) = 2\pi\sqrt{2L}/\sqrt{(2M+1)\cdot\pi\cdot a\cdot g} \qquad (1)$$

where M is the mode number, L, the shelf width, a, the shelf slope, and g, the acceleration due to gravity. The shallow shelf regions in Monterey Bay extend roughly from Monterey Harbor to Moss Landing and out to the southern rim of MSC in the southern half of the bay, and from Moss Landing

up to Santa Cruz out to the northern rim MSC in the northern half of the bay (Fig. 1). We have selected a representative range of values for *L* and *a* for the first two edge wave modes (*M*=0 and *M*=1) and plotted *T(M,L,a)* in each case (Fig. 8). For a shelf width of 5 km and a shelf slope of 0.01, for example, we obtain predicted edge wave periods in the range of 23–42 minutes. These wave periods are well within the range of periods associated with the natural oscillations of Monterey Bay and so energy trapping in the form of edge waves may occur and thus contribute to the arrival sequence observed in Figs. 4 and 7. However, we note that the extent to which energy trapping contributes to edge wave activity in Monterey Bay their occurrence will be restricted to the near shore regions and so our ability to observe them will depend strongly on location.
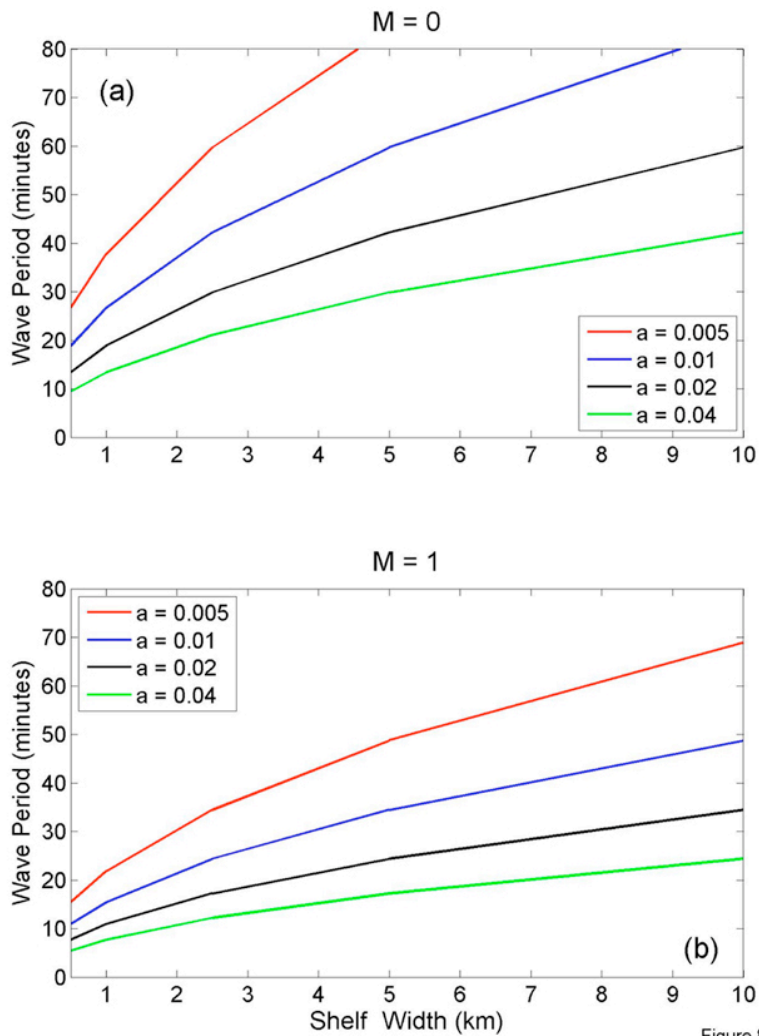

Figure 8. The predicted wave periods (in minutes) are shown for edge wave modes M = 0 in the top panel (a), and M = 1 in the lower panel (b). The wave periods are plotted as a function of shelf width in km along the abscissa, and bottom slope (*a*) for slopes of 0.005 (red), 0.01 (blue), 0.02 (black), and 0.04 (green).

4. DISCUSSION

Although the tsunamis generated by the Great Alaskan Earthquake of 1964 and the Chilean earthquake of 2010 both entered Monterey Bay across its mouth, the response to each event was quite different. In the first case, the Great Alaskan Earthquake excited only one mode, the first transverse mode of oscillation for Monterey Bay with a well-documented period of approximately 36 minutes consistent with quarter wave resonance. In the second case, the Chilean earthquake of 2010 excited several modes including the first longitudinal mode with a period in the neighborhood of 55 minutes. Both SSA and EEMD revealed this mode. SSA also revealed what is most likely the first transverse mode of oscillation with a period of 34-35 minutes although this mode was not detected in the EEMD decomposition. An oscillation with a period of 26-27 minutes was also detected in the SSA decomposition but its true nature has not been firmly established. Finally, both SSA and EEMD revealed an often-observed oscillation with a period of 21-22 minutes.

The tsunamis associated with the Great Alaskan Earthquake and the Chilean Earthquake both entered Monterey Bay from offshore but arrived from opposite directions. Unlike the Great Alaskan Earthquake, which excited only one resonant mode inside the bay, the Chilean Earthquake excited several modes. The bay's response to these two tsunamis was very different and must be related to the manner in which the tsunami-generated waves associated with these events entered the bay. First, as discussed by Defant (1961), the period of the longest free oscillation that enters an embayment is expected to increase significantly for embayments with relatively wide entrances. For a simple rectangular bay with a flat bottom where the width of the entrance is equal to its length, the period will be increased by approximately 37%. For Monterey Bay, the width of the entrance actually exceeds the distance between the entrance and Moss Landing by at least 35% and so considerable period lengthening is expected. Also, the shape of the entrance to an embayment has a great effect on the period of incoming free oscillations, according to Defant (1961). The shape of the entrance to Monterey Bay is somewhat asymmetric due to the presence of the Monterey Peninsula at the southern end of the bay (Fig. 1). Breaker and Broenkow (1994) found that poleward propagating disturbances along the coast took almost 5 days to travel from a point approximately 10km north of Pt. Sur on the open coast (Fig. 1) to a point located inside the bay at its southern extremity, suggesting that propagating waves from the south take a rather circuitous path into the bay. Conversely, incoming waves from the north should enter the bay via a more direct path where the coastline is less obstructed. Further, according to Murty (1984), the direction from which a tsunami approaches the entrance to a bay determines to a large extent the amplitudes, frequencies, and phases of the oscillations inside the bay. As a result we expect that there will be a preferred direction for which maximum amplitudes of the resonant modes inside the bay will occur. Thus, we conclude that (1) the period of incoming tsunami-generated waves (regardless of the direction from which they arrive) will be increased significantly due to the relatively wide entrance, (2) the asymmetric shape of the entrance to Monterey Bay may affect the periods of incoming tsunami-generated waves differently for those that enter the bay from the south than for those that enter from the north, and (3), the directions of the incoming waves were most likely different in each case.

The Great Chilean or Valdivia Earthquake of May 22, 1960 was the most powerful earthquake ever recorded, measuring 9.5 on the moment magnitude scale. It generated a tsunami that affected most of the greater Pacific basin from Chile to Alaska. However, we have no record of this event in

Monterey Bay, since, to our knowledge, no tide gauge was in operation at that time. Because the epicenter of the Valdivia Earthquake was located along the coast of Chile similar to the Chilean earthquake of 2010, although several hundred km further south, the seiche modes excited by this event in Monterey Bay may have been similar although the amplitudes were most likely much higher and the arrival sequence may have lasted longer.

Next we consider the seiche mode whose period is approximately 27 minutes. It roughly corresponds to the third mode of oscillation predicted by WHK with a period of 28 minutes but its corresponding spatial pattern was confined to the southern half of the bay, not consistent with subsequent bay-wide observations at this frequency. According to Lynch (1970), an oscillation with a period of 27 minutes could correspond to a shelf wave, and results from this study suggest that energy trapping in the shallow shelf areas of Monterey Bay could lead to the formation of edge waves with periods of this order. However, Breaker et al. (2008), using EEMD applied to water levels in Elkhorn Slough detected modes of oscillation with periods of approximately 55, 36, 27, and 22 minutes using conventional spectral analysis but did not detect an oscillation with a period of 27 minutes using EEMD. This result is consistent with our results from this study using EEMD. As discussed in Huang et al. (1998), because EEMD is not based on Fourier methods of decomposition, the energy associated with nonlinearities in the data is not represented by harmonics but takes a different form.[3] Thus, the question arises as to whether a spectral maximum with a period of approximately 27 minutes represents a fundamental oscillation or simply a harmonic? Based on our experience with EEMD we favor the latter explanation.

Finally, different results were obtained using SSA and EEMD. SSA detected oscillations with periods of 52-57 minutes, 34-35 minutes, 26-27 minutes, and 21-22 minutes, whereas EEMD detected oscillations with periods of 50-55, and 21-22 minutes. The slight differences in the first case can most likely be attributed to measurement uncertainties. These uncertainties include actual changes in the period of oscillation dependent on where in the arrival sequence the measurements were made, uncertainties due to the sampling interval, and finally, differences due to bandwidth considerations. Although the results of EEMD did not reproduce an oscillation in the range of 34-35 minutes, in our past experience in comparing these methods, we have detected certain oscillations using EEMD that were not detected using SSA and so, in our view, the jury is still out on whether one method is inherently better than the other in its ability to resolve different oscillations. As discussed above, SSA detected an oscillation with a period in the range of 26-27 minutes but its reality is seriously in doubt. Finally, both methods detected an oscillation with a period of 21-22 minutes.

5. SUMMARY AND CONCLUSIONS

The purpose of this study has been to extract the primary frequencies contained in the arrival sequence produced by the tsunami from the Chilean earthquake of 2010 in order to determine what

---

[3] Breaker et al. (2008) found that the energy associated with harmonics in conventional spectral analysis appeared to be rather uniformly distributed across a broad range of frequencies in the corresponding EEMD analysis based on the Hilbert spectrum.

natural oscillations or seiche modes were generated in Monterey Bay. Two methods of spectral decomposition, Singular Spectrum Analysis (SSA) and Ensemble Empirical Mode Decomposition (EEMD), were employed to extract the frequencies of interest and provided a useful basis for comparison. Although the amplitudes of the tsunami-generated signals were small in comparison to the semidiurnal and diurnal tides, by using SSA and EEMD we were able to effectively separate the signals of interest for detailed examination. The wave train associated with of the Chilean tsunami lasted for at least four days in Monterey Bay due to several processes. It was concluded that although reflections may not have contributed significantly to the arrival sequence, secondary undulations, and energy trapping in the form of edge waves, most likely did contribute to the tsunami-related arrivals.

The results of the SSA decomposition resolved oscillations with periods of 52-57, 34-35, 26-27, and 21-22 minutes, all frequencies that have been predicted and/or observed in previous studies. The results of the EEMD decomposition only detected oscillations with periods of 50-55, and 21-22 minutes. Periods in the range of 50-57 minutes were somewhat variable due to measurement uncertainties but almost certainly correspond to the first longitudinal mode of oscillation for Monterey Bay (e.g., Breaker et al., 2010). Periods in the range of 34-35 minutes correspond to the first transverse mode of oscillation that assumes a nodal line across the entrance of the bay. A period of approximately 37 minutes, close to the period of 34-35 minutes observed in this study, was observed from the Great Alaskan Earthquake of 1964 in Monterey Bay and most likely represents the same mode of oscillation. A period in the range of 26-27 minutes, although previously observed, does not necessarily represent a fundamental mode (Breaker et al., 2008), and a period in the range of 21-22 minutes has been predicted and observed on several occasions (e.g., Lynch, 1970). The tsunamis associated with the Great Alaskan Earthquake and the Chilean Earthquake both entered Monterey Bay from offshore but from opposite directions. Unlike the Great Alaskan Earthquake, which excited only one resonant mode inside the bay, the Chilean Earthquake excited several modes suggesting that the asymmetric shape of the entrance to the bay was an important factor, and that the directions of the incoming tsunami-generated waves were most likely different.

Finally, the results from SSA and EEMD produced somewhat different results. Although a period of 34-35 minutes was observed in the results from SSA, it was not detected in the results from EEMD. However, in previous comparisons between the two methods we have observed that oscillations detected in EEMD were not obtained using SSA. SSA also revealed an oscillation with a period of 26-27 minutes, not observed in the results from EEMD. As pointed out above, however, this oscillation may not represent a fundamental mode but instead may be harmonically related to the first longitudinal mode of oscillation whose period is approximately 55 minutes. Overall, both methods have been helpful in interpreting the results of this study.

REFERENCES

Breaker, L.C., and W.W. Broenkow (1994), The circulation of Monterey Bay and related processes. Oceanography and Marine Biology: an Annual Review, 32, 1-64.

Breaker, L.C., W.W. Broenkow, W.E. Watson, and Y.-H. Jo (2008), Tidal and non-tidal oscillations in Elkhorn Slough, California. Estuaries and Coasts, 31, 239 – 257.

Breaker, L.C., T.S. Murty, J.G. Norton, and D. Carroll (2009), Comparing the sea level response at Monterey, California to the Loma Prieta Earthquake of 1989 and the Great Alaskan Earthquake of 1964.   Science of Tsunami Hazards, 28, 255 - 271.

Breaker, L.C., Y.-H. Tseng, and X. Wang (2010), On the natural oscillations of   Monterey Bay: observations, modeling, and origins. Progress in Oceanography, 86, 380-395, doi: 10:1016/j.pocean.2010.06.001.

Camfield, F.E. (1980), Tsunami Engineering. Special Report No. 6. U.S. Army, Corps of Engineers, Coastal Engineering Research Center, Fort   Belvoir, VA, 222 pp.

Defant, A. (1961), Physical Oceanography: Volume II. The MacMillan   Company, New York.

Flandrin P., G. Rilling G, and P. Concalves (2004), Empirical mode decomposition as a filter bank. IEEE Signal Processing Letters, 11, 112 – 114.

Ghil, M., M.D. Allen, K. Dettinger, D. Kondrashow, M.E. Mann, A.W. Robertson, A. Saunders, Y. Tian, F. Varadi, and P. Yiou (2002), Advanced spectral methods for climatic time series. Reviews of Geophysics, 40, 1003, 3-1 – 3-41.

Golyandina, N., V. Nekrutkin, and A. Zhigljavsky (2001), Analysis of Time Series Structure: SSA and Related Techniques. Monographs on Statistics and Applied Probability 90. Chapman & Hall/CRC, Boca Raton.

Huang, N.E., and others (1998), The empirical mode decomposition and the Hilbert spectrum for nonlinear and non-stationary time series analysis. Proceedings of the Royal Society of London A, 454, 903- 995.

Huang, N.E. (2005a), Introduction to the Hilbert-Huang Transform and its related mathematical problems, p. 1-24. In: Huang NE, Shen SSP (eds) Hilbert-Huang Transform and its applications, Interdisciplinary Mathematical Sciences - Vol. 5. World Scientific, New Jersey.

Huang, N.E. (2005b), Introduction to the Hilbert-Huang Transform and some recent developments,. In: Huang NE, Attoh-Okine NO (eds) Hilbert-Huang Transform in Engineering. Taylor & Francis, Boca Raton. pp 1-24.

Jenkins, G.M., and D.G. Watts (1968), Spectral Analysis and its Applications. Holden-Day, San Francisco.

Kowalik, Z., and T.S. Murty (1993), Numerical Modeling of Ocean Dynamics. World Scientific, Singapore.

Lynch, T.J. (1970), Long wave study of Monterey Bay. M.S. Thesis, Naval Postgraduate School, Monterey, California.

MacMahan, J.H., J.H. Reniers, E.B. Thornton, and T.P. Stanton (2004a), Infragravity rip current pulsations. Journal of Geophysical Research, 109, C01033, doi: 10.1029/2003JC002068.

MacMahan, J.H., J.H. Reniers, E.B. Thornton, and T.P. Stanton (2004b), Surf zone eddies coupled with rip current morphology. Journal of Geophysical Research, 109, C07004, doi: 10.1029/2003JC002083.

Murty, T. S. (1984), Storm Surges – Meteorological Ocean Tides. Bulletin Number 212. Canadian Journal of Aquatic Sciences, 897 pages.

Murty, T.S., N. Nirupama, I. Nistor, and A.D. Rao (2005), Role of trapped and leaky modes around Andaman and Nicobar Islands: Tsunami of 26 December 2004. Proceedings of the National Workshop on Tsunami Effects and Mitigation Measures, Allied Publishers Pvt. Ltd., Chennai, pp. 3-21.

Murty, T.S., U. Aswathanarayana, and N. Nirupama (2006), The Indian Ocean Tsunami. Taylor & Francis, London.

Murty, T.S., N.P. Kurian, and M. Baba (2008), Roles of reflection, energy, trapping and secondary undulations in the tsunami on Kerala coast. International Journal of Ecology & Development, 10, 100-114.

Nakano, M. (1932), Preliminary note on the accumulation and dissipation of the energy of secondary undulations in a bay. Proc. Phys. Math. Soc. Japan, SER 3, 44-56.

Peel M.C., G.E. Amirthanathan, G.G.S. Pegram, T.A.McMahon, and F.H.S. Chiew (2005), Issues with the application of Empirical Mode Decomposition analysis. In: Zerger, A., Argent R.M. (eds) MODSIM 2005 International Congress on Modelling and Simulation, Modelling and Simulation Society of Australia and New Zealand, December 2005, pp 1681-1687.

Preisendorfer, R.W. (1988), Principal Component Analysis in Meteorology and Oceanography. Elsevier, Amsterdam.

United States Geological Survey (2010), USGS, Earthquake Hazards Program (March 6, 2010). "10-Degree Map Centered at 35S, 75W".

Vautard, R., P. Yiou, and M Ghil (1992), Singular-spectrum analysis: A toolkit for short, noisy chaotic signals. Physica D, 58, 95-126.

Wilson, B.W., J.A. Hendrickson, and R.E. Kilmer (1965), Feasibility study for a   surge - action model of Monterey, California. U.S. Army Corps of Engineers, Waterways Experiment Station, Vicksburg, MS, 166 pp.

Wilson, B. W. , L. M. Webb, and J. A. Hendrickson (1962), The nature of tsunamis: Their generation and dispersion in water of finite depth. NESCO Technical Report No. SN 57-2, National Engineering Science Company.

Wu, Z., and N. E. Huang (2009), Ensemble empirical mode decomposition: A noise-assisted data analysis method. Advances in Adaptive Data Analysis, 1, 1 – 41.

Yanuma, T. , and Y. Tsuji (1998), Observations of edge waves trapped on the continental shelf in the vicinity of Makurazaki Harbour, Kyushu, Japan. Jour. Oceanog., 54, 9-18.

APPENDIX A − SINGULAR SPECTRUM ANALYSIS

Singular Spectrum Analysis (SSA) is a method of spectral decomposition that is similar in many respects to Principal Component Analysis (e.g., Preisendorfer, 1988). According to Golyandina et al. (2001), the general purpose of SSA is to decompose a time series into a sum of a small number of interpretable components or modes such as a slowly varying trend, oscillatory components and "structureless"noise. The data adaptive nature of the basis functions that are employed in SSA make the method suitable for analyzing data that may be nonlinear and/or non-stationary. SSA can be applied to relatively short, noisy time series (e.g., Vautard et al., 1992), making it well suited for analyzing the data employed in this study.

To perform SSA, a multidimensional time series called the trajectory matrix is initially formed from the original one-dimensional time series. The dimension of this matrix is called the window length, L. As stated by Ghil et al. (2002), this process is equivalent to representing the behavior of the system by a succession overlapping views of the series through a sliding window whose length is equal to L. The trajectory matrix can be formed from a univariate time series in several ways. The approach we use leads to a Toeplitz trajectory matrix. A Toeplitz matrix is symmetric and has the property of being diagonally-constant with dimensions in this case of $L \times L$. To construct a Toeplitz trajectory matrix, the lagged covariances, S_{ij}, for a time series x_t, , $t = 1,2,.......,N$, are calculated according to

$$S_{ij} = \frac{1}{N - |i - j|} \sum_{t=1}^{N-|i-j|} x_{|i-j|+t} x_t \qquad (1a)$$

where we have centered the record by first removing the mean. S_{ij} is equivalent to the unbiased version of the autocovariance function due to the normalization that is employed (Jenkins and Watts, 1968). The resulting matrix, S, at this point can be decomposed into eigenvalues, λ_k and eigenvectors, e_k, according to

$$\Lambda = E^T S E \qquad (2a)$$

where E is the diagonalizing matrix whose columns contain the eigenvectors, E^T, its transpose, and the elements of the diagonal matrix, Λ, contain the eigenvalues. When the square roots of the eigenvalues or singular values are plotted in descending order, the so-called "singular spectrum" is obtained. The principal components, a_k, can be obtained by projecting the time series onto each eigenvector as

$$a_t^k = \sum_{j=1}^{L} x_{t+j} e_j^k \qquad (3a)$$

where $t = 1,2,....,N$, and e_j^k represents the jth component of the kth eigenvector, and the number of principal components that are produced is equal to $N - L + 1$.

The principal components represent moving averages or filtered versions of the original series, x_t .

Finally, the original times series can be recovered by calculating the reconstructed components (Vautard et al., 1992). The kth reconstructed component can be calculated according to

$$r_t^k = \frac{1}{F_t} \sum_{j=G_t}^{H_t} a_{t-j+1}^k e_j^k \qquad (4a)$$

where the lower and upper limits of summation, G_t and H_t , and the normalizing factor, F_t , depend on location within the time series. Following Ghil et al. (2002), the normalizing factor, $F_t = 1/t$, for $1 \leq t \leq L\text{-}1$, $1/L$, for $L \leq t \leq N - L + 1$, and $1/N\text{-}t+1$, for $N - L + 2 \leq t \leq N$. The lower limit, $G_t = 1$, for $1 \leq t \leq L\text{-}1$, 1, for $L \leq t \leq N - L + 1$, and $t\text{-}N+M$, for $N - L + 2 \leq t \leq N$. The upper limit, $H_t = t$, for $1 \leq t \leq L\text{-}1$, L, for $L \leq t \leq N - L + 1$, and L, for $N - L + 2 \leq t \leq N$. Unlike the principal components which have length $N - L + 1$, the reconstructed components have length N, equal to that of the original time series. These components correspond to partial time series and when summed over all modes reproduce the original time series within the accuracy of the calculations.

APPENDIX B – EMPIRICAL MODE DECOMPOSITION

The method we employ is referred to as Empirical Mode Decomposition and Hilbert Spectral Analysis, or EMD/HSA. More concisely, EMD/HSA is called the Hilbert-Huang Transform, or simply the HHT. The methodology is described in detail by Huang et al. (1998), Huang (2005a), and Huang (2005b). Unlike SSA which has a formal mathematical basis, EEMD is empirically based thus emphasizing the inherent differences in these methods.

In this study we focus on that portion of the methodology that involves EMD. EMD is a method of decomposing a time series into a sequence of empirically orthogonal Intrinsic Mode Function (IMF) components and a residual. The method is similar to Singular Spectrum Analysis (Golyandina et al., 2001). However, in EMD, the number of modes is determined by the data whereas in Singular Spectrum Analysis (SSA), the number of modes is determined by the user. EMD is data adaptive, and, in contrast to Fourier spectral decomposition, it does not require stationarity of the data. As such, it is well-suited for the analysis of non-stationary and nonlinear time series. The IMF components are often physically meaningful because the characteristic scales in each case are determined by the data itself. As in SSA, selected modes may require grouping in order to extract a physical basis. A number of recent studies have examined EMD in detail (Flandrin et al., 2004; Peel et al., 2005; Huang, 2005a; Huang, 2005b).[1]

Each IMF represents a mode of oscillation with time-dependent amplitude and frequencies that lie within a narrow band, the center of which defines the mean period of the mode. The process of extracting the individual modes or essential scales from the data is called sifting and is performed

---

[1] The last two references refer to texts that contain chapters by various authors.

many times to produce a single IMF. In this process local maxima and minima are identified in the record and envelopes are formed by fitting cubic splines to the extreme values. The differences between the envelope and the mean provide an estimate of the first IMF component. Once the first IMF, imf_1, has been obtained, it is subtracted from the original data, $x(t)$, producing residuals, r_1, which can be expressed as

$$x(t) - imf_1 = r_1 . \qquad (1b)$$

The residuals, r_1, are then subjected to the same process, yielding the second IMF, imf_2, as

$$r_2 = r_1 - imf_2 , \qquad (2b)$$

and so on, until a final residual is obtained that often corresponds to a long-term trend in the data.

One problem in the application of EMD is that mode mixing occurs when a time series includes intermittently occurring signals of widely separated time scales, i.e., when a high-frequency signal in one time interval is followed by a smooth, low frequency signal in the following time interval. To address this problem, Wu and Huang (2009) have developed a noise-assisted technique called "ensemble EMD", or EEMD, which defines the true IMF as the mean of an ensemble of IMFs. An ensemble member consists of the signal plus white noise. By creating an ensemble of IMFs, it is possible to generate IMFs, each of which has a narrow frequency band, that essentially do not overlap with the frequencies that are contained in adjacent IMFs. In applying the technique, the white noise that is added to the signal according to

$$x_i(t) = x(t) + \varepsilon_i(t) \qquad (3b)$$

where $x(t)$ represents the ith observation, $x_i(t)$ represents the ith observation perturbed by white noise, and $\varepsilon_i(t)$ represents the white noise that is added to the ith observation. The amplitude of the added noise, $\varepsilon_i(t)$, can be calculated as the ratio of the standard deviation of the added noise to that of the input data. In our case we have used a value of 0.1, but we also initially used values of 0.05 and 0.20, and obtained similar results in each case. Typically, the number of realizations or ensemble size is several hundred in order to obtain $x_i(t)$. In the present study we used an ensemble size of 300 in each case. Finally, the maximum number of IMFs that can be generated from a given data set is approximately given by $Log_2(N)$, where N represents the total number of observations in the record. This upper limit is based on the fact that the number of zero-crossings from one IMF to the next decreases by a factor that is approximately one half. In practice, however, somewhat fewer IMFs are usually produced.
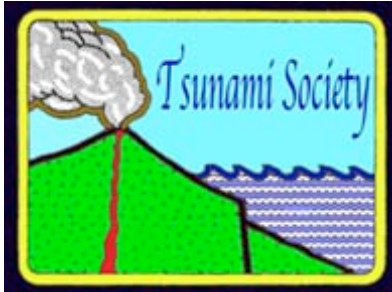
THE TSUNAMIS OF JANUARY 3, 2009 IN INDONESIA AND OF JANUARY 15, 2009 IN SIMUSHIR AS RECORDED IN THE SOUTH KURIL ISLANDS

**G.V. Shevchenko[1], A.G. Chernov[2], P.D. Kovalev[3], D.P. Kovalev[4], O.N. Likhacheva[5].,
A.V.Loskutov[6] and A.A. Shishkin[7]**

[1] Head, Tsunami Laboratory, Inst. Marine Geology and Geophysics FEB RAS, Yuzhno-Sakhalinsk, Russia
[2] Researcher, Nyzniy Novgorod State Technical University, Nizniy Novgorod, Russia
[3] Head, Wave Processes Laboratory, Inst. Marine Geology and Geophysics FEB RAS, Yuzhno-Sakhalinsk, Russia
[4] Researcher, Inst. Marine Geology and Geophysics FEB RAS, Yuzhno-Sakhalinsk, Russia
[5] Vice-director, Inst. Marine Geology and Geophysics FEB RAS, Yuzhno-Sakhalinsk, Russia
[6] Researcher, Inst. Marine Geology and Geophysics FEB RAS, Yuzhno-Sakhalinsk, Russia
[7] Leading Engineer, Inst. Marine Geology and Geophysics FEB RAS, Yuzhno-Sakhalinsk, Russia

ABSTRACT

Bottom pressure gauges installed by the Institute of Marine Geology & Geophysics RAS in Shikotan Island, Kitoviy Bay (Iturup Is.) and near Cape Van der Linde (Urup Is.), recorded two tsunamis during the month of January 2009. The first of the recorded tsunamis was generated by the January 3, 2009 earthquake in Indonesia and the second by the January 15, 2009 Simushir Island earthquake in the nearby seismic zone of the South Kuril Islands. The two tsunamis were additionally recorded by tide gauges at Hanasaki (Hokkaido Is.) and Malokurilskaya Bay (Shikotan Is.), but with considerable delay of the Indonesian tsunami from its estimated time of arrival. The tsunami travel time delay can be attributed to effects of energy trapping by Japan's continental shelf. The maximum height of the Simushir tsunami (97 cm in the Kitoviy Bay) was also observed much later than the arrival of the first wave. Totally, the oscillations lasted for about 32 hours, which is very long time period for the relatively weak tsunami. The present study investigates these apparent anomalies of the

long wave oscillations and whether they were caused by reflected waves from the original earthquake or from a secondary tsunami generated by a weaker aftershock.

1. INTRODUCTION

In July 2008, the Marine Geology & Geophysics Institute of the Far East Branch of the Russian Academy of Sciences installed bottom pressure gauges in Shikotan Island, near Cape Lovtsov (on the north-eastern part of Kunashir Island), in Kitoviy Bay (of Iturup Island) and near Cape Van-der-Lind and Cape Kastrikum (Urup Island)(Fig. 1). The specific purpose for the installation was to record tsunamis originating close to the South Kuril Islands active seismic zone and to study long wave spectra variability depending on weather conditions.
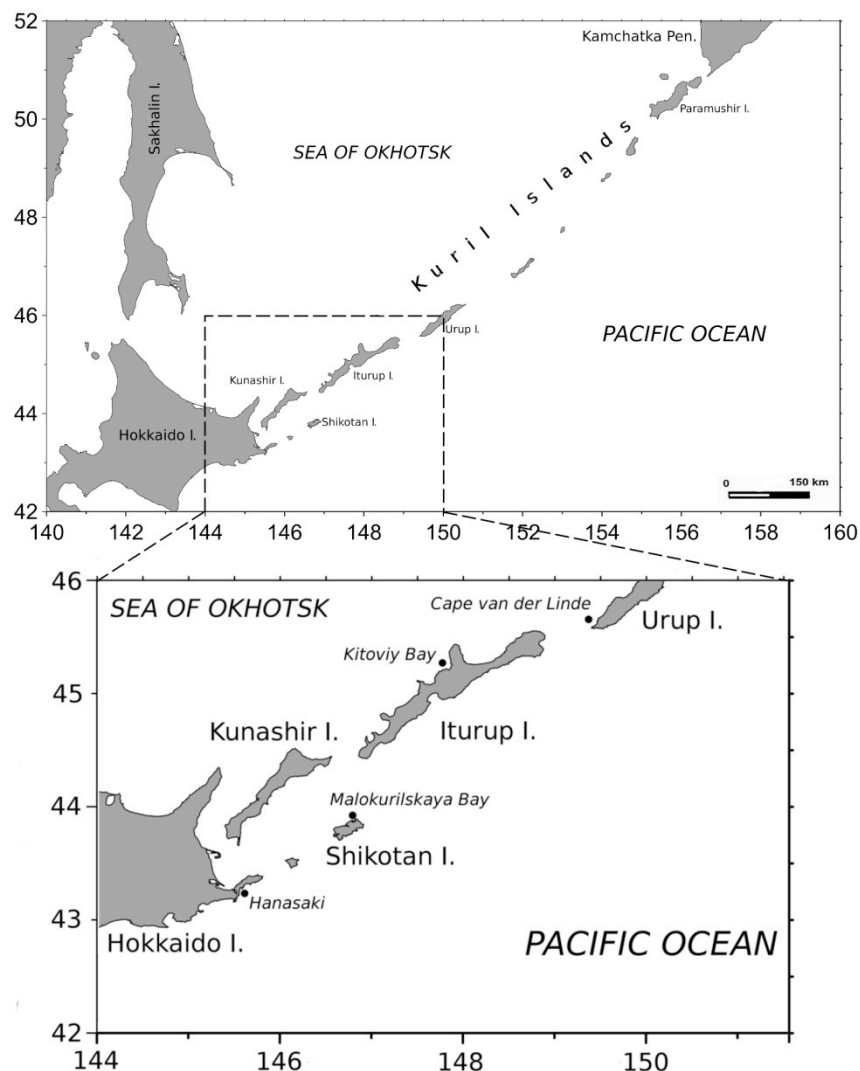
Figure 1. Location of gauges in South Kuril Islands

Measurements taken at these gauges had a sampling interval of 1 second, thus enabling the recording of heights and periods of both long period waves and wind waves. The methodology for converting bottom pressure measurements of wind generated surface wave heights has been developed and documented (Kabatchenko et al, 2007).

Bottom pressure gauges were used previously to record waves in the tsunami frequency range on the shelf and on the Kuril Islands continental slope (Zhak and Soloviev, 1971). The first offshore tsunami record was obtained on the shelf of Shikotan Island on February 23, 1980 (Dykhan *et al.*, 1981). This recording indicated a significant tsunami transformation in the near shore zone in comparison to the deep-sea region.

Autonomous bottom gauges were utilized to measure the hydrostatic pressure changes associated with sea level oscillations. Each gauge had a battery with enough power to continuously record for more than 180 days. In order to suppress energetic high-frequency swell and wind wave oscillations and avoid possible aliasing, a Kaizer-Bessel filter was used. One-minute data samples were collected filtered and archived. The forecasted tidal fluctuation was subtracted from the one-minute sea level time series. The residual series were subsequently analyzed to identify tsunami fluctuations or other anomalous long wave oscillations induced by weather related activity (typhoons, thunderstorms, squalls or abrupt atmospheric pressure jumps). The spectra of extreme events were compared with the background spectra, which corresponded to normal weather conditions.

The autonomous gauges were picked up and re-installed again in October 2008. The first phase of the experiment did not provide the anticipated results because only one weak tsunami and wave activity from one weak storm were recorded (Levin et al, 2009). However, during the next phase, which lasted from October 2008 to April 2009, more significant data was recorded – even though the two gauges installed near Cape Lovtsova and Cape Kastrikum were lost.

Records were obtained for two tsunamis during that period. The first of these was the tsunami of 3 January 2009, which originated in Indonesia and the second was the tsunami of 15 January 2009, which was generated by an earthquake in the nearby Simushir Island. Additionally, records were obtained for waves generated by several strong winter storms. The remotely generated tsunami from Indonesia was clearly evident in the Malokurilskaya gauge (Shikotan Harbor). However, this tsunami could not be identified in records from the other pressure gauge stations. Gauges in Malokurilskaya Bay, Kitoviy Bay and the gauge near Cape Van-der-Lind recorded the tsunami generated in nearby Simushir Island. All stations on January 23-24, 2009, recorded anomalous sea level oscillations resembling those of tsunami signal although no known strong earthquakes had occurred on these days anywhere in the Pacific and none was included in the NEIC's catalogue of seismic events. More than likely the recorded event was of meteorological origin (a "meteorological tsunami"). The present paper provides an analysis of the above events with emphasis on the tsunami of 15 January generated in nearby Simushir Island.

2. THE INDONESIAN TSUNAMI OF JANUARY 3, 2009

A major earthquake with moment magnitude Mw=7.6 (USGS) occurred near Irian Jaya in Indonesia at 19:43 UTC on January 03, 2009. Its epicenter was at 0.5º S; 132.8º E, about 93 miles WNW from Manoewari (Irian Haya) and its depth was 34.7 km (USGS). The quake generated a significant tsunami, which was recorded by tide gauges along southeastern Asia and Japan. The

estimated and observed tsunami arrival times, as well as wave heights for various points of Pacific were given at NOAA's website http://wcatwc.arh.noaa.gov/about/tsunamimain.php.

Most of the tsunami's energy propagated in a northward direction. The first waves reached Kyushu Island in Japan in approximately 4 hours after the quake's origin time (Fig. 2). The tsunami waves continued toward the South Kuril Islands, reaching Shikotan Island about three hours later. As expected there was attenuation with distance and the amplitude of the waves decreased by the time they reached Shikotan. Although the tsunami wave heights were not even high close to Indonesia, there were appreciable tsunami fluctuations recorded by the Shikotan Island gauge. The unusual fluctuations were puzzling and required further detailed consideration and investigation.
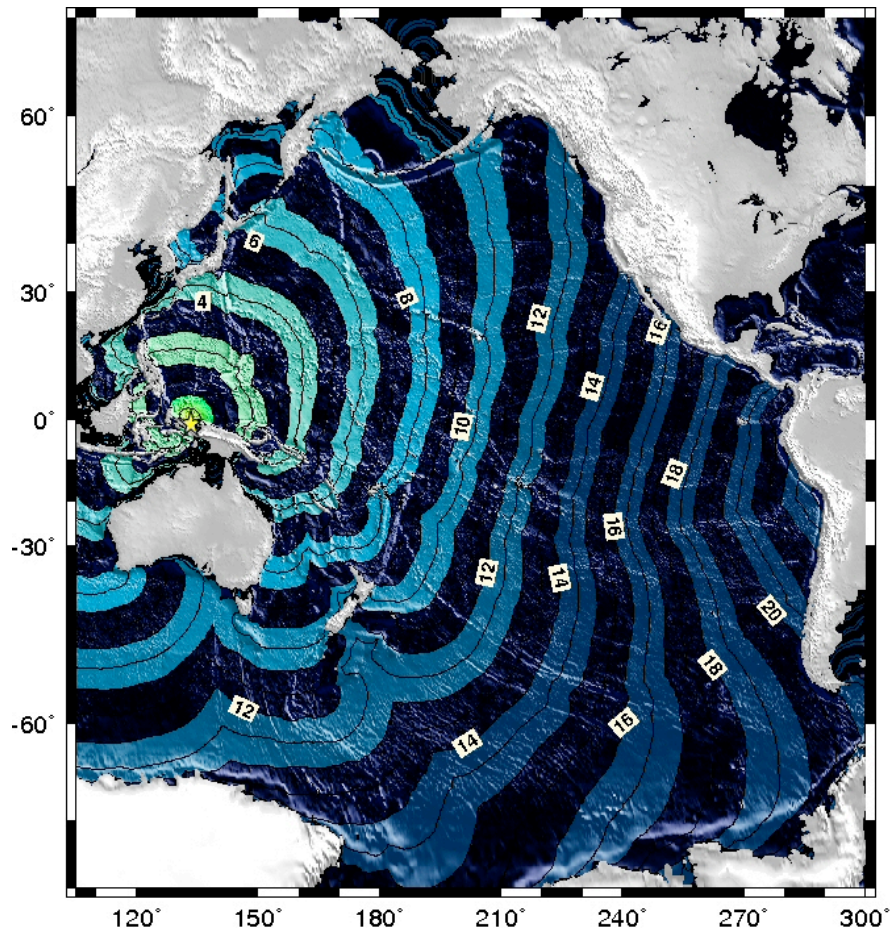
Figure 2. Calculated time travel map of Indonesia (Irian Jaya) tsunami (from NOAA website).

Daily segments of sea level recording of the January 2009 Indonesia tsunami were obtained from the gauges at Malokurilskaya Bay and from Hanasaki, as shown in Fig. 3. However, the tsunami could not be identified from records of gauges located at Kitoviy Bay and near Cape Van-der-Lind. The gauge at Malokurilskaya recorded a series of a well-distinguished group of waves with average

periods of 18-19 min that corresponds to the zeroth (Helmholth) mode of the bay resonant oscillations (Djumagaliev et al, 1994). Such oscillations are routinely observed in the bay, so it is difficult to identify accurately the arrival time of the weak tsunami at this station.

Nevertheless, certain change in the character of fluctuations is noticed since 4:12 (UTC) was the most probable time of tsunami arrival at Malokurilskaya Bay. The maximum height (12 cm) in the first group of five waves was that of the fifth wave. Weak fluctuations were also observed after the first group within about an hour.

The first of the tsunami waves recorded at 6:48 of January 4th (UTC). Subsequently, about 10 fluctuations were recorded with an average period of 18 minutes and approximately identical heights (from a crest to trough) ranging from 17-19 cms. The apparent tsunami wave activity lasted for about 3 hours. At 9:00 UTC, the intensity of long-wave variations decreased to the background average level. According to NOAA's chart the tsunami travel time to Shikotan Island from the source region was 7.5 hours and the estimated time of wave arrival (ETA) was at about 3:10 – which was approximately four 4 hours ahead of the observed tsunami arrival. This is a point that needs special review. The NOAA website specified the ETA at Hanasaki stations to be at 3:05 (UTC) (see fig. 2). This estimate is approximately an hour sooner than that recorded at Malokurilskaya Bay, which was compatible with the numerical model calculation.
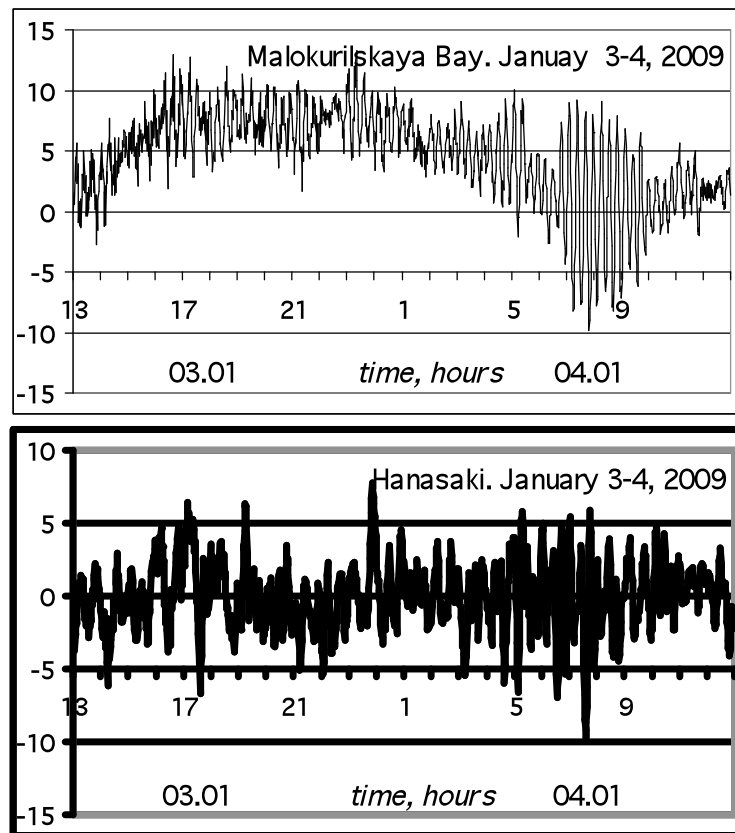

Figure 3. Residual (de-tided) sea level records (cm) in Malokurilskaya Bay and in Hanasaki (Hokkaido, Japan) from 13:00 on January 3 through 13:00 on January 4 (UTC).

The better-identified group of waves with periods 19-20 minutes was observed in this location about 2 hours later. The strongest fluctuation was observed at 7:37 (UTC) at the end of the wave group.

In order to determine the spectral properties of long wave oscillations recorded at each of the gauges, power spectral analyses were performed for two different data segments - both of one day's duration. The first analysis of the records was conducted for the day prior to the tsunami arrival and that was identified as "normal" and selected as being the background. The second analysis was on the records of the "tsunami period" that included the observed tsunami oscillations. Spectral analysis of the record from the Malokurilskaya Bay record represents the tsunami-caused amplification of resonant oscillations with a period of 18-19 minutes in comparison to the high-frequency oscillations (Fig. 4a). For example, values of spectral density on the resonant periods of 3.3 and 4 min were apparently decreased by tenfold – which was in good agreement with the visually observable "pure" signal of the tsunami.
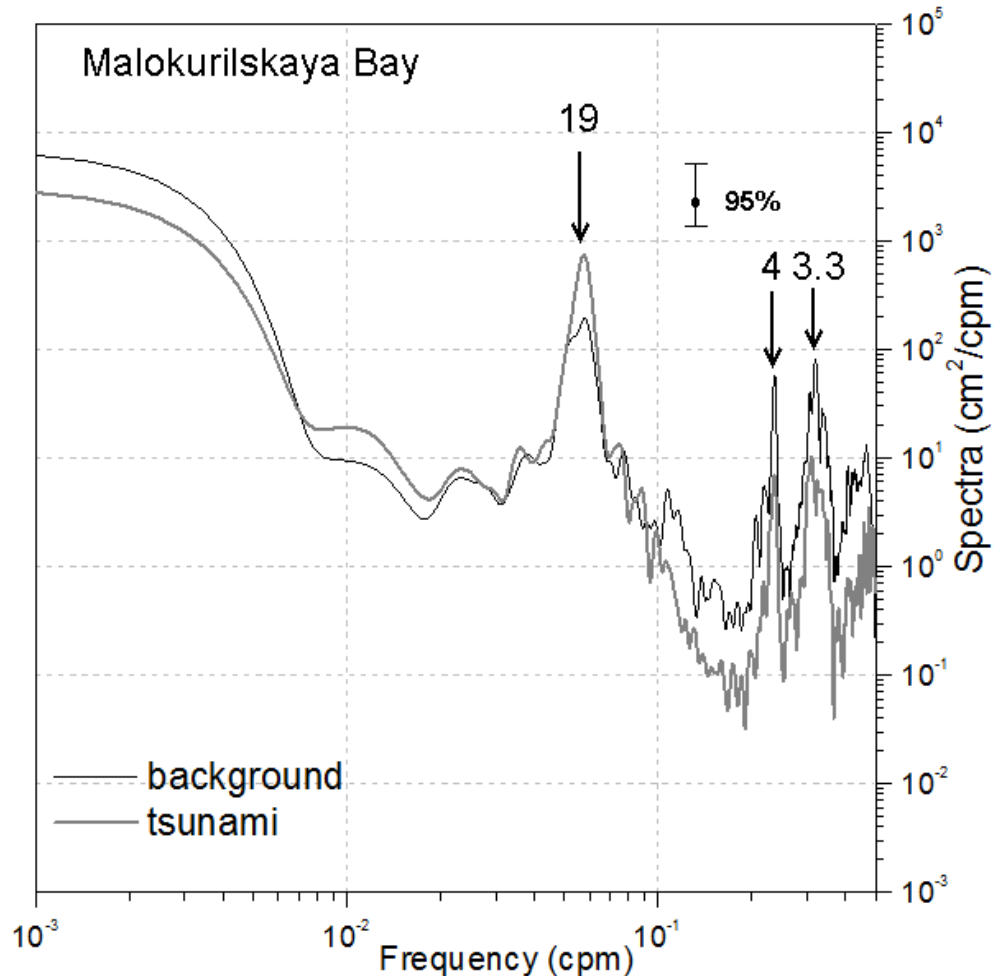

Figure 4a. Spectra of background and Indonesia tsunami-caused sea level oscillations in the Malokurilskaya Bay, Shikotan Island.

The Hanasaki station record shows that the tsunami caused significant amplification of the bay's resonant oscillations that had average periods of about 15 minutes. Also, maximum heights occurred on the bay's resonant oscillations that had periods of 19 and 35 minutes - which were absent in the background spectrum (Fig. 4b).

More than likely, the observed wave processes were caused by tsunami energy trapping and better energy retention by edge waves propagating on the shelf along the coast of Japan and traveling much slower than the long waves traveling in the open ocean (3 times deeper). The estimated time of wave front propagation along the coast of Japan - without considering the trapping effect - is about 2 hours. For the group of edge waves the estimated delay is about 4 hours and that corresponds to the actual observations.

The wave group period on the shelf of Japan and the resonant period near Malokurilskaya Bay were the reason of the clearly evident recording of the Indonesian tsunami in spite of its distant source. The edge waves did not reach the gauges near the Iturup and Urup Islands, so this was the probable reason that the Indonesian tsunami could not be identified in those records.
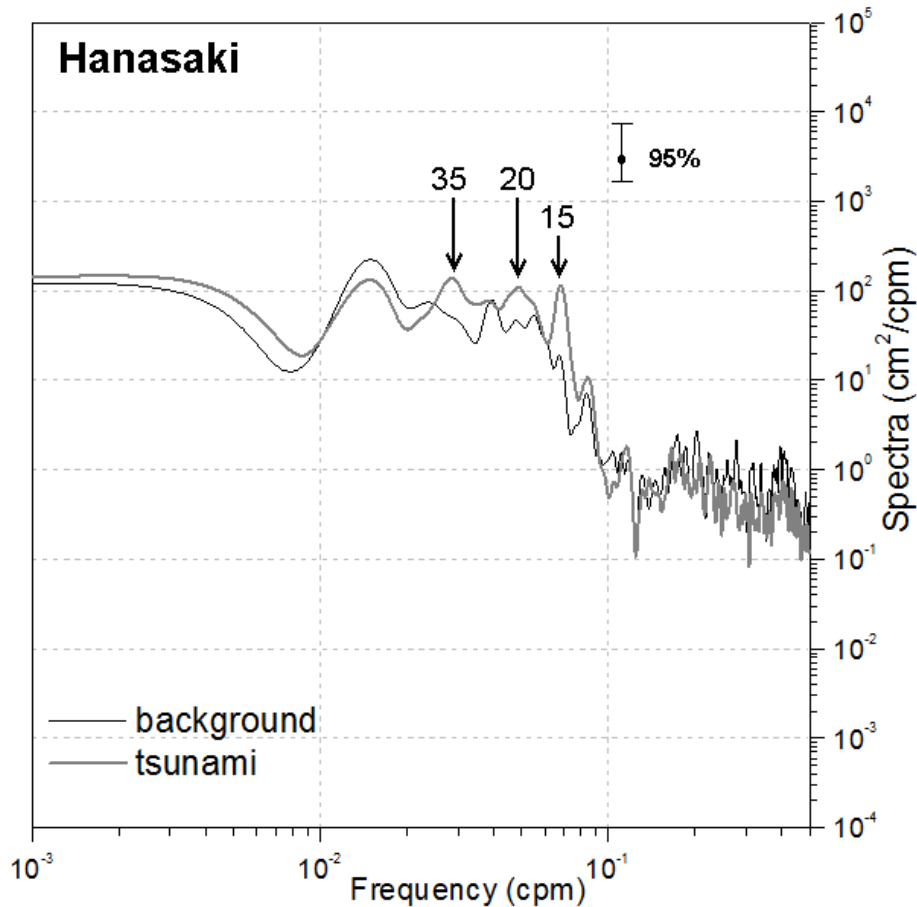
Figure 4b. Spectra of background and Indonesia tsunami-caused sea level oscillations. Hanasaki station, Hokkaido Island.

3. THE SIMUSHIR TSUNAMI OF JANUARY 15, 2009

At 17:49 UTC on 15 January 2009, a shallow earthquake (36.0 km depth) with moment magnitude (M=7.4, USGS) occurred in nearby Simushir Island. Its epicenter was at 46.9º S, 155.2º E - about 270 miles south from Severo-Kurilsk, Kuril Islands close to where the Simushir January 13, 2007 earthquake had occurred. (Fig. 5). Although similar in magnitude to the earthquake in Indonesia the 15 January Simushir event generated only a weak local tsunami.
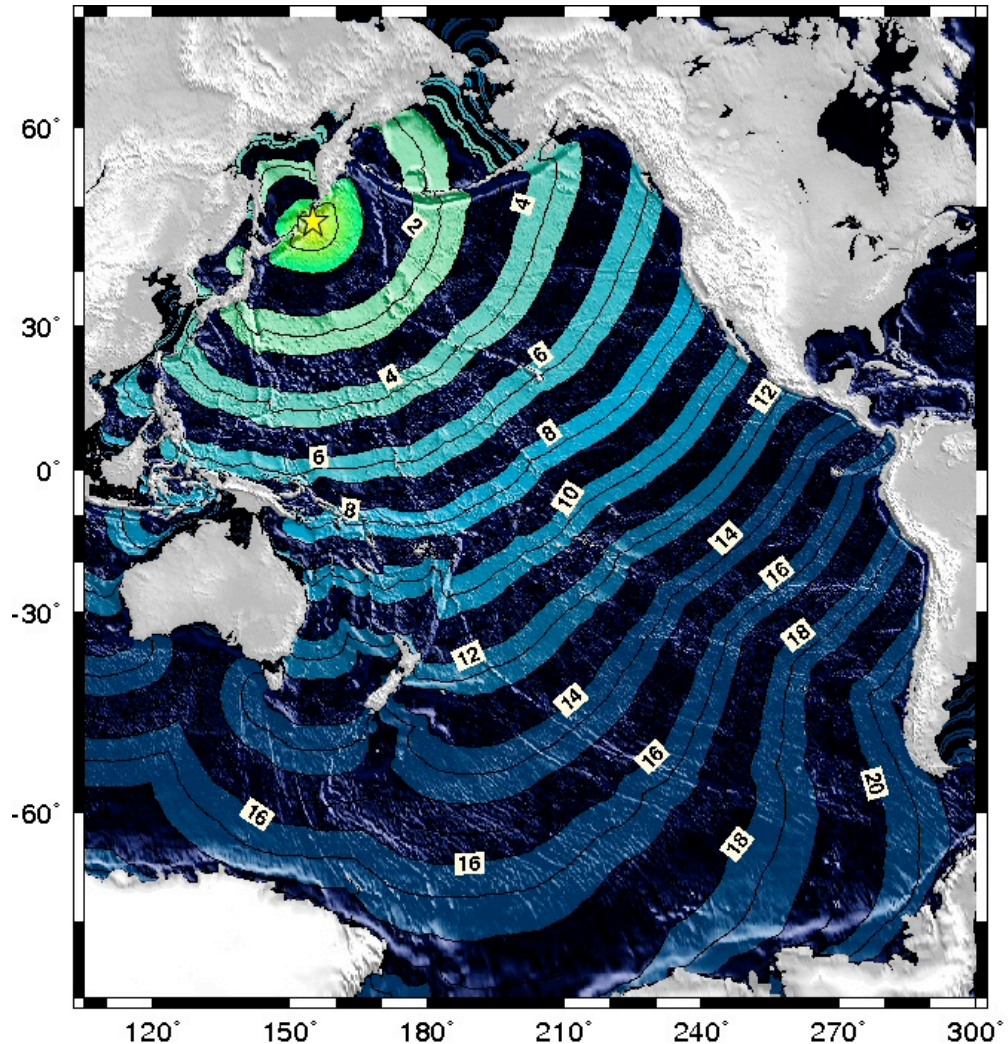

Figure 5. Tsunami Travel time chart of the January 15, 2009 tsunami (NOAA graphic).

According to NOAA modeling, the main energy flux of the tsunami was directed to the deep area of Pacific Ocean (Fig. 6). However, a significant portion of the tsunami wave energy was directed towards the Sea of Okhotsk. Similar wave energy distribution had been observed with two other tsunamis generated in November 2006 and January 2007 near Simushir Island.
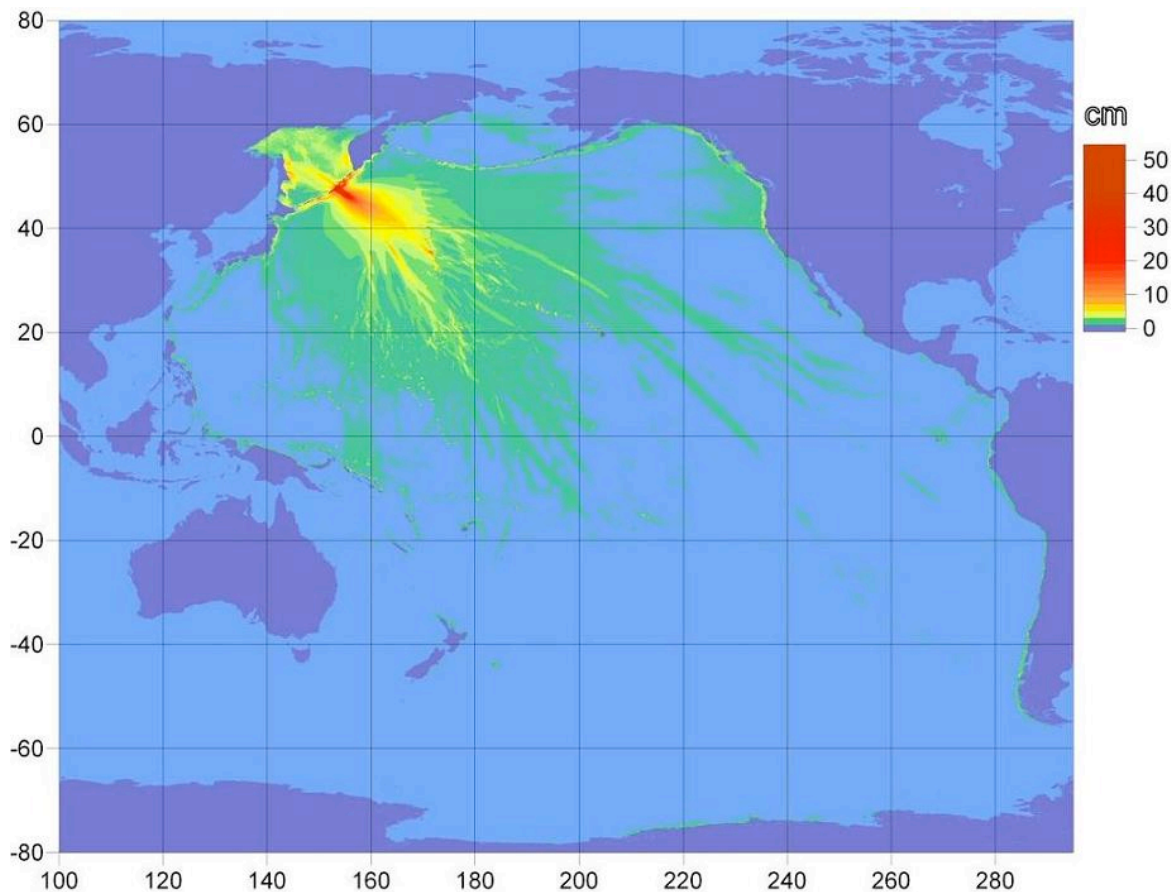
Figure 6. Calculated maximum amplitude graph of the Simushir tsunami (from NOAA website).

The tsunami waves were recorded on the bottom pressure gauges in Malokurilskaya Bay, in Kitoviy Bay and near Cape Van-der-Lind (Fig. 7).

Very high noise levels prevented the determination of tsunami wave arrival and recording of wave amplitudes at the last two stations. The background noise was caused by severe storms related to cyclone movement during that time period. Spectral estimates of wind waves for 12-hour intervals showed increasing energy at periods of 8-10 seconds to two orders of magnitude in comparison with the calm weather (Fig. 8). The maximum intensity of wind waves occurred in the first half of January 16. At that time the storm center was located near Simushir Island (Fig. 9), far from Shikotan Island and so the influence of the storm at Malokrilskaya Bay was not as powerful. Thus the tsunami was clearly recorded as a group of waves with periods of about 19 minutes and amplitudes ranging from 10-11 cms. The first wave of the group was recorded at 23:56 UTC and the duration of subsequent intense oscillations lasted for about 4 hours. Like with the Indonesian tsunami, the determination of Simushir tsunami arrival time at the Malokurilskaya Bay was complicated. Most probably, the ETA was 20:11 UTC, thus the tsunami travel time from the source area to the gauge at this bay was about 2 hours and 20 minutes – which was consistent with the estimated travel time of the Simushir tsunami of January 13, 2007 (Rabinovich et al, 2008; Lobkovsky et al, 2009)
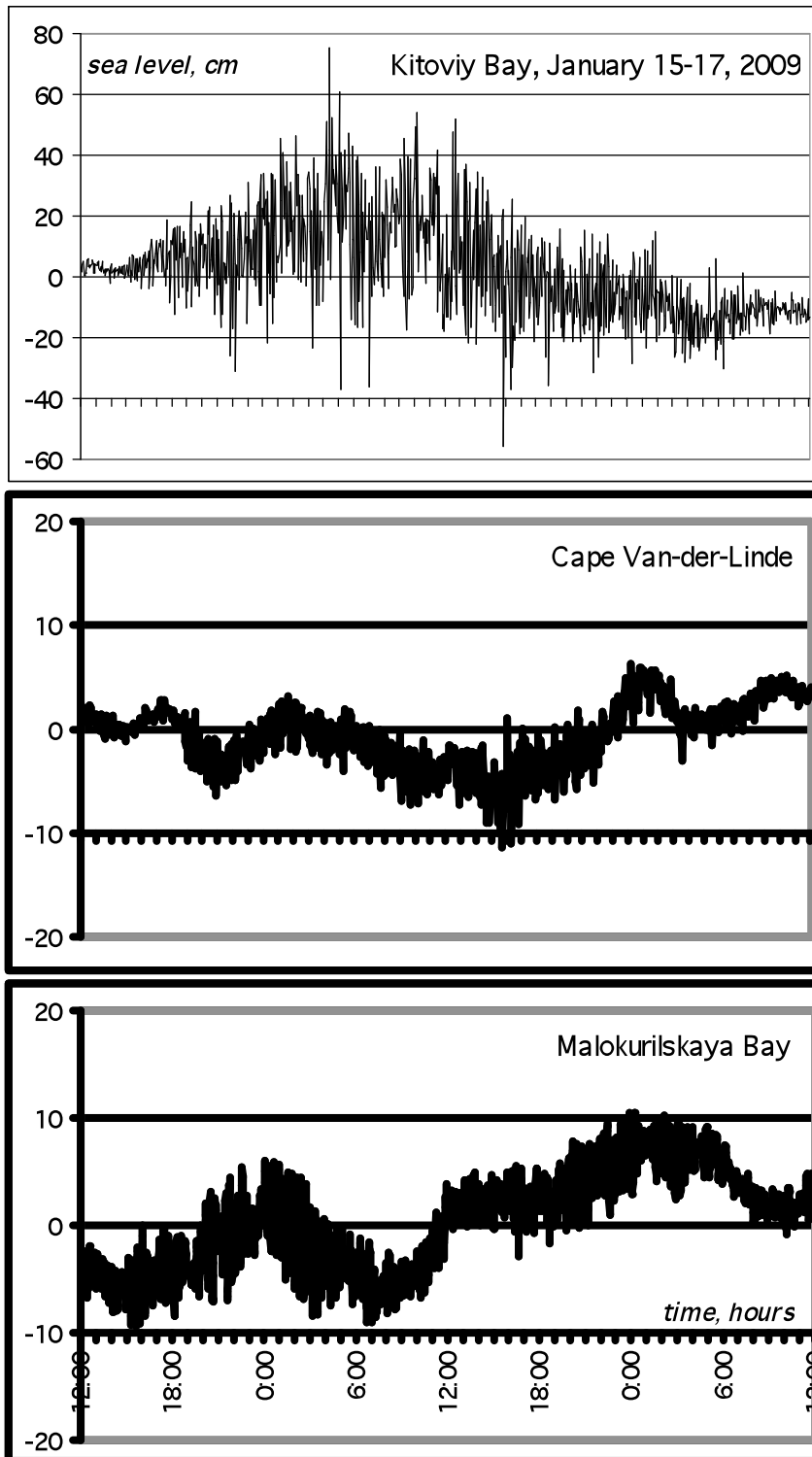
Figure 7. Residual (de-tided) records (in cms) from 12:00 on January 15 through 12:00 on January 17 (UTC) at stations at Kitovy Bay, Cape Van der Linde and Malokurilskaya Bay.
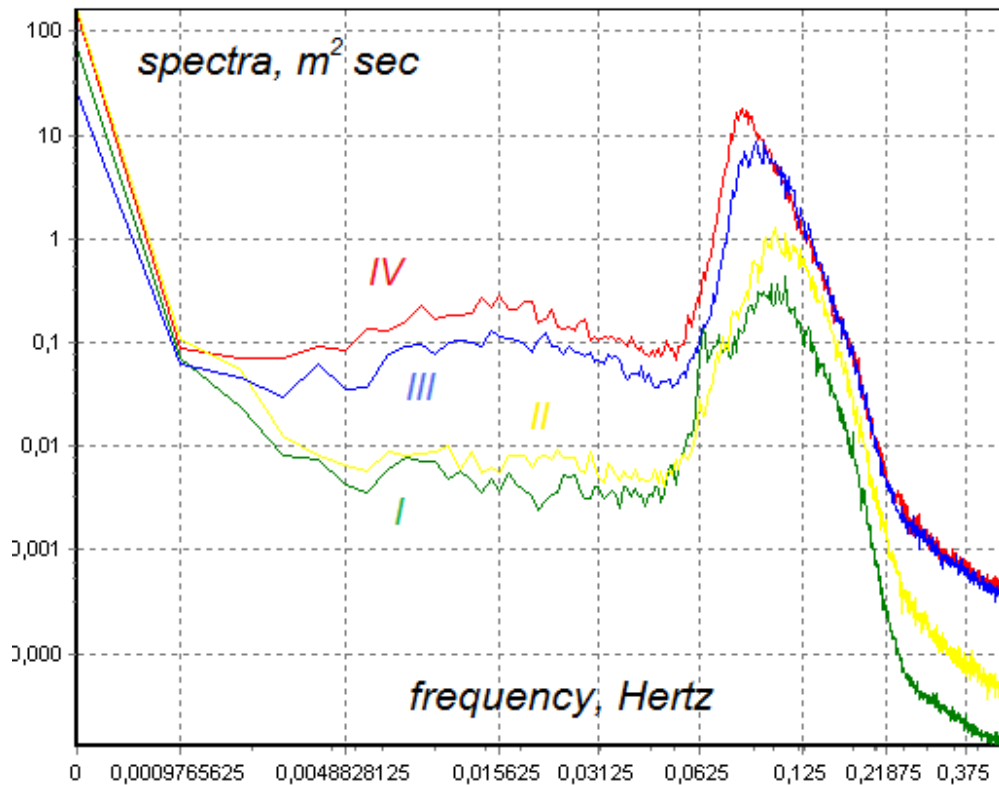
Figure 8. Wind waves spectra calculated for different time segments at the Cape Van der Linde gauge: a) from 0:00 to 12:00 on January 15 (I); b) from 12:00 to 24:00 on January 15 (II); c) from 0:00 to 12:00 on January 15 (I);   d) from 12:00 to 24:00 on January 15 (II); e) from 0:00 to 12:00 on January 16 (III); f) from 12:00 to 24:00 on January 16 (IV).

For the tsunami of November 15, 2006, which was generated in the same general region, the maximum wave arrived 3 hours and 50 minutes after the first tsunami arrival. The delay was attributed to energy trapping by the shelf effect (Rabinovich et al, 2008). Similarly, the delay of the group of waves in 2009 can be attributed to the same effect.

To estimate the arrival time of the tsunami and of the wave height, we were forced to use averaging with a 3-minute time window. For the Cape Van der Linde record that was enough to suppress the high-frequency noise and determine exactly the characteristics of the tsunami. The arrival time of first wave was 18:49 UTC, one hour after the earthquake. The maximal wave heights ranging from 8-10 cms were observed much later, on January 16 from 15:43 to 16:49 UTC. The oscillations lasted for about 32 hours, which is a very long time for the weak tsunami. The arrival of waves with a maximum height a day after the earthquake was also very unusual. In the Malokurilskaya Bay, there was an increase of zeroth mode of resonant oscillations since 19:20. Probable reasons for these lasting wave oscillations can be either the arrival of reflected waves or the generation of more tsunami waves by subsequent strong aftershocks.
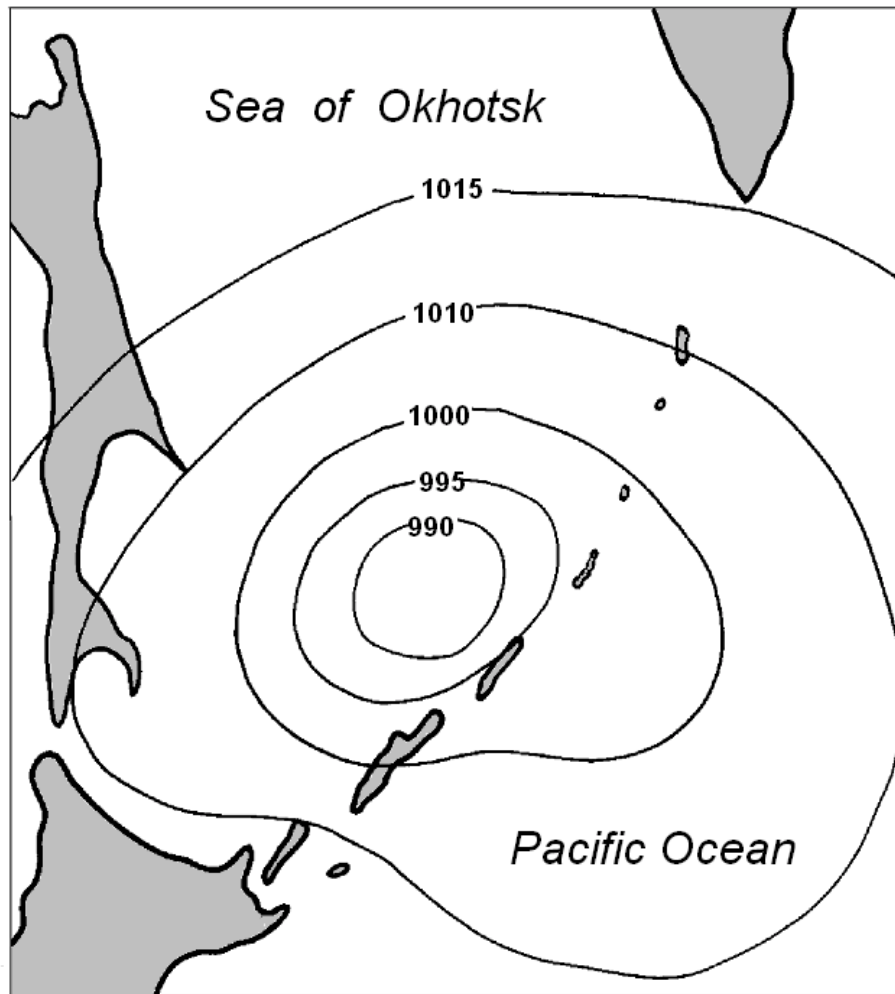
Figure 9. Atmospheric pressure spatial distribution from the weather map of Sakhalin hidrometeorological agency on January 16, 2009, 00:00 UTC.

 The Sakhalin Department of Geophysical Survey (RAS) recorded two strong aftershocks on January 16. The first occurred at 15:14 UTC and had magnitude M=5.8 (preliminary estimate. Its epicenter was south of the main quake at 46.1 N, 155.9 E. The second occurred at 16:48, had a magnitude of M=5.9 and its epicenter was east of the main quake at 46.9 N, 155.8 E. It is difficult to evaluate the probability of tsunami generation by these aftershocks since the seismic information was not sufficient.
 On the other hand, the probability of reflected waves influence is also low, since the tsunami was weak and the main flux of the wave energy was directed toward the open ocean. In view of these considerations the anomalous structure of the tsunami-caused oscillations, which could not be adequately explain.

More anomalous wave structure was observed in Kitoviy Bay and this can be related to certain superimposition of low- and high-frequency oscillations (Fig. 10a). Tsunami wave tsunami arrival time on this station could not be determined. The amplitude of long waves increased sharply since 15:27 UTC, about two hours before the earthquake. The reason of the increasing sea level oscillations was the strong cyclone in the area, which had a central pressure of 985 millibars. In the second half of January 15 the cyclone was over the Sea of Okhotsk near Iturup Island. The orientation of isobars indicated the direction of the wind toward Kitoviy Bay. The cyclone caused a severe storm in the port of Kurilsk, where the spectral energy of wind waves was amplified by about 200 times. The probability of the tsunami arriving concurrently with a strong storm is very small, since each of them is a rare event.
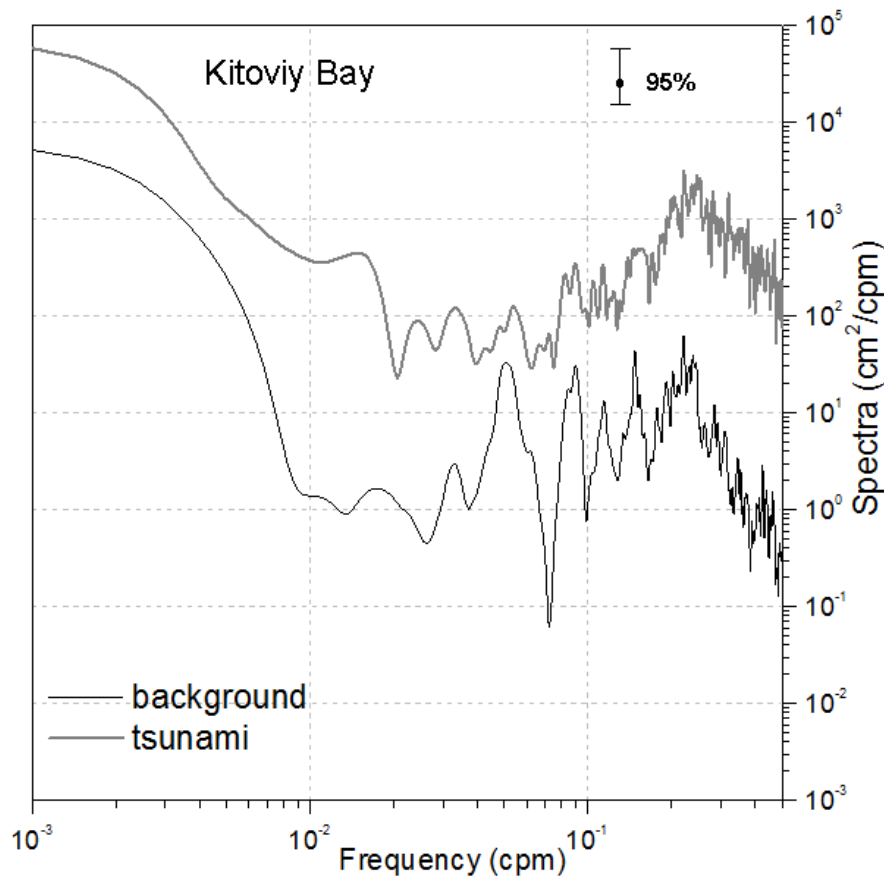

Figure 10a. Spectra of sea level oscillations of the background and of the Simushir tsunami at Kitoviy Bay, Iturup Island.

The intensity of sea level oscillations had steadily increased by 5:00 on January 16, when a maximum height of about 97 cms was recorded; A significant sea level lowering (ebb wave) can be seen in Figure 4. The high amplitude sea level fluctuations continued until 12:40. Another amplification of oscillations was recorded at 15:50, about the same time when the maximum waves arrived at the Cape Van der Linde gauge station. Decrease in the long wave intensity to a background level of occurred on January 17 at about 9:00.

The calculation of the spectra for the background signal and the tsunami-caused oscillations was performed in the same manner as for the Indonesian tsunami. The results are illustrated in Figure 6. In the Malokurilskaya Bay there was considerable distinctions in the energy level between the tsunami and the background spectra at the period of main resonant mode (18-19 min) and for the low frequency band at the periods 45-60 min. In contrast, the Cap Van der Linde gauge record analysis shows a significant increase in the tsunami spectra in the high frequency band (for periods less then 6 min) (Fig. 10b). Most probably, this increase was caused by the storm's action and not by the tsunami.
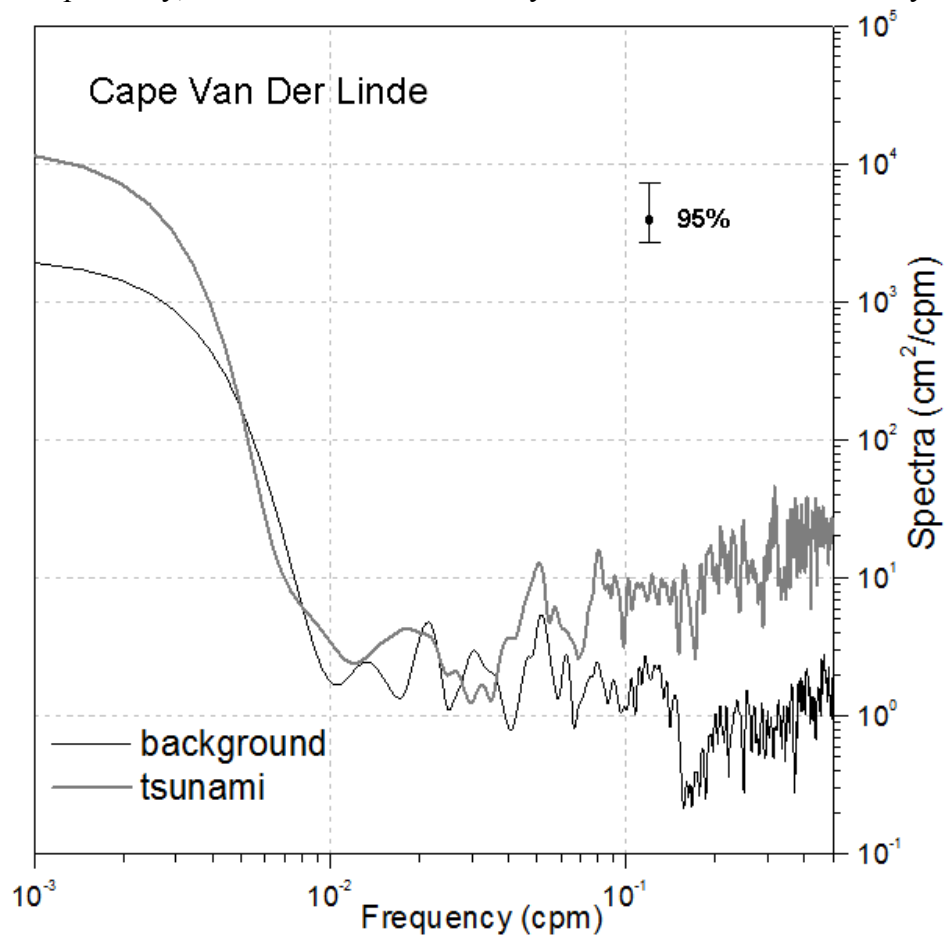

Figure 10b. Spectra of background and Simushir tsunami caused sea level oscillations. Van der Linde gauge, Urup Island.

The tsunami caused an increase of the main spectral peaks with periods of 12 and 20 minutes. These peaks were observed also in the background spectra in the first segment of the experiment and were related also to the influence of shelf resonance in the area (Levin et al, 2009).

The most significant distinctions in energy level of the tsunami and the background spectra were observed almost for the entire frequency band of the Kitoviy Bay record. The most significant increase in energy was found in the both high- and low-frequency bands of the spectrum (at the periods less than 5 min and 30-60 min). The energy increase in the high-frequency band was caused

by the strong storm. The increase in energy fluctuations at low frequencies (although weaker) was observed at other stations as well.

Several well-expressed peaks in the spectra of background signal were found, which corresponded to the Kitoviy Bay resonant modes; however they were weakly expressed in the spectra of the tsunami. The most significant peak was observed in the 20-minute period. In contrast to the gauge recordings at Malokurilskaya Bay (Fig. 10c) and at Cape Van der Linde, energy increases in this period was found to be weak in Kitoviy Bay. What cause these differences is not known.
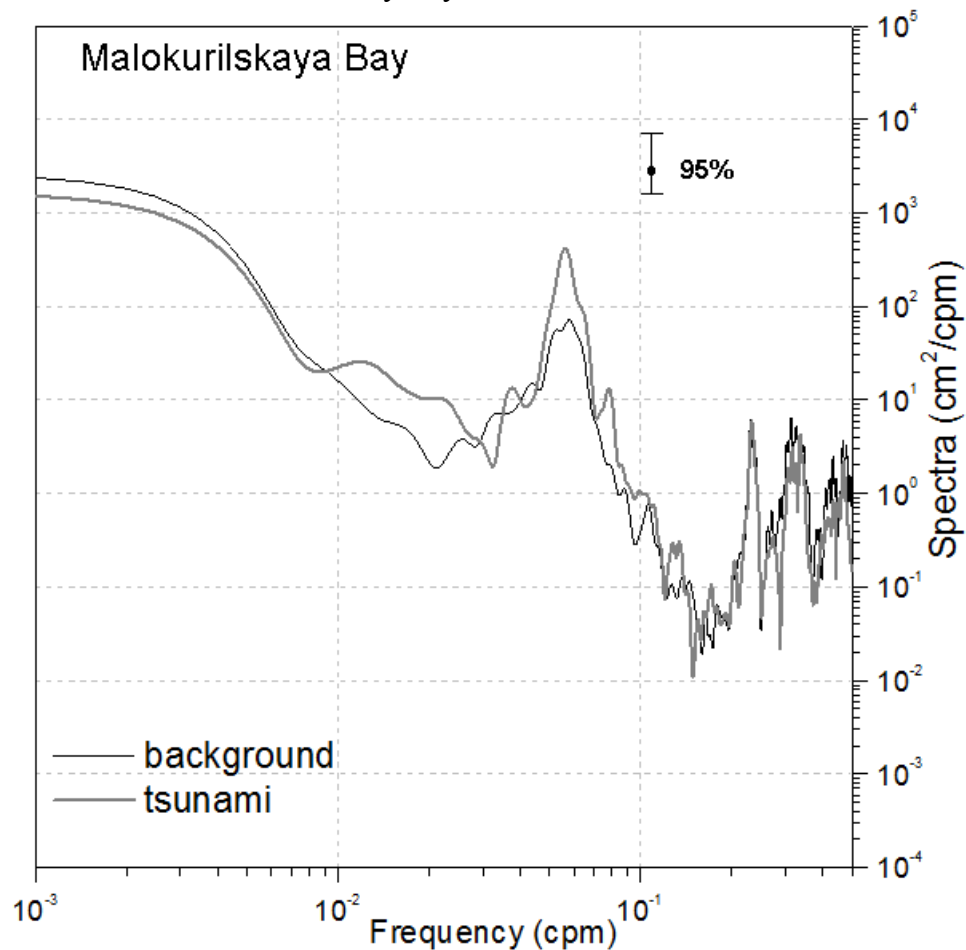

Figure 10c. Spectra of background and the Simushir tsunami as recorded at the Malokurilskaya Bay, Shikotan Island.

4. METEOROLOGICAL TSUNAMI OF JANUARY 23-24, 2009

All the autonomous gauges recorded the anomalous sea level oscillations on January 23-24, 2009. De-tided sea level records from 0:00 January 22 through 24:00 on January 24 are shown in Figure 11. These oscillations were found to be similar to tsunami signal, in particular to the above shown Simushir tsunami. However, there was no report in the NEIC seismological catalogue showing any strong earthquakes in the Pacific area on that day. More than likely, the recorded event was

caused by meteorological forces (a "meteorological tsunami"). However, there were no observations of any cyclones in the area of South Kuril Islands during that period and only atmospheric fronts were observed.
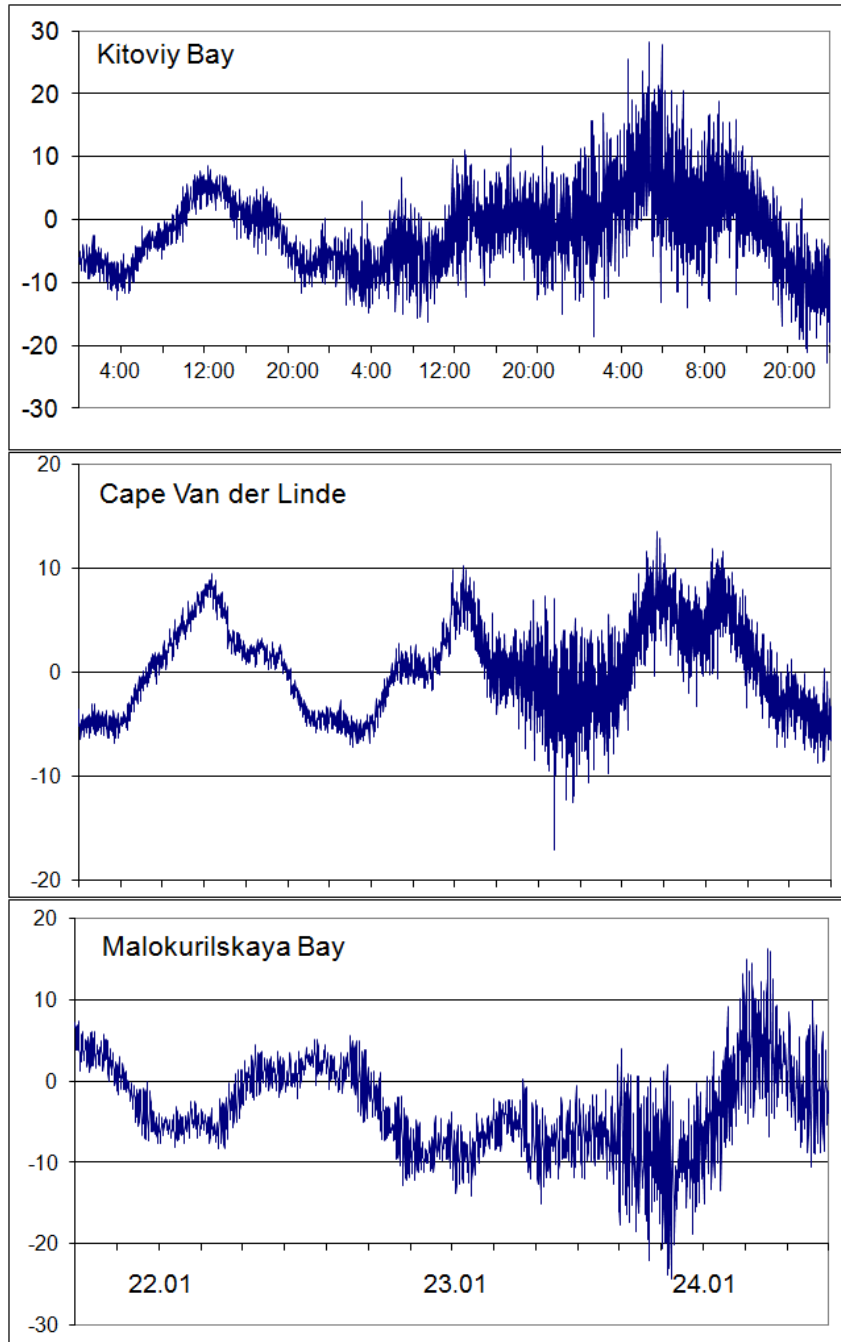

Figure 11. Residual (de-tided) sea level records (in cms) of gauge stations at Kitovy Bay, Cape Van der Linde and Malokurilskaya Bay from 0:00 of January 22 through 24:00 of January 24 (UTC).

The Kitoviy Bay gauge recorded the strongest oscillations. Increases in the amplitudes began on Jan.23 from 1:20 UTC. The most intense oscillations were observed on January 24 from 1:10 till 13:20. As with the records of the Simushir tsunami, both high-and low-frequency oscillations were manifested on January 23-24. During this period, the amplitude reached 10-12 cms. Considerable distinctions in the energy level between the assumed meteorological tsunami and the background spectra were observed almost in the entire frequency band (Fig. 12a).
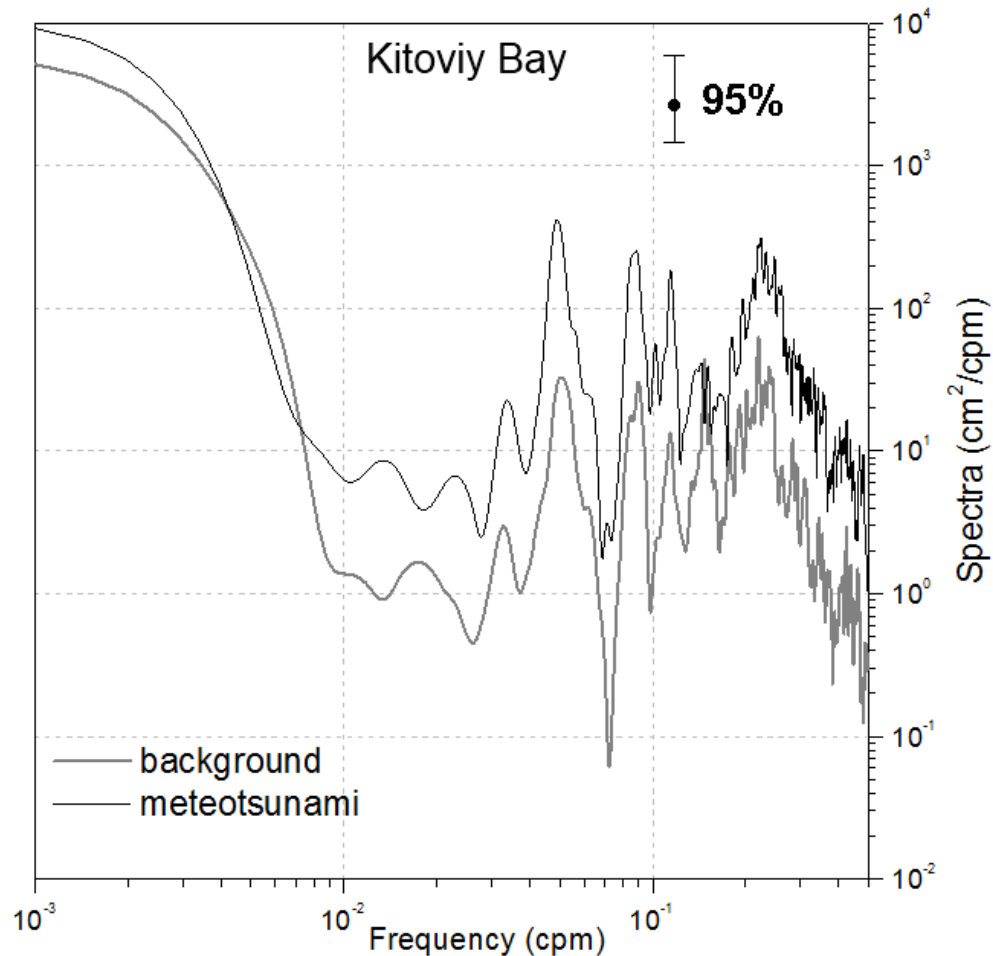

Figure 12a. Spectra of background and presumed meteorological tsunami oscillations in Kitoviy Bay, Iturup Island.

In contrast to the above shown record of the Simushir tsunami, all resonant peaks were found to be well expressed in the spectra of meteorological tsunami. The most significant increase (more than an order of magnitude) was observed at the main peak with a period of about 19 minutes.

At the Cape Van der Linde station the increase in amplitude began significantly later than in Kitoviy Bay. It occurred on January 23 beginning at 11:40 UTC. The most intense sea level oscillations were observed from 19:30 on Jan. 23 until 2:40 on January 24. During this period, the

amplitude reached 7-8 cms. Spectra of the presumed meteorological tsunami were similar to the spectra of the Simushir tsunami. Considerable distinctions in the energy level between meteorological tsunami and the background spectra were observed almost for the entire frequency band, especially in the high frequency band (Fig. 12.b).
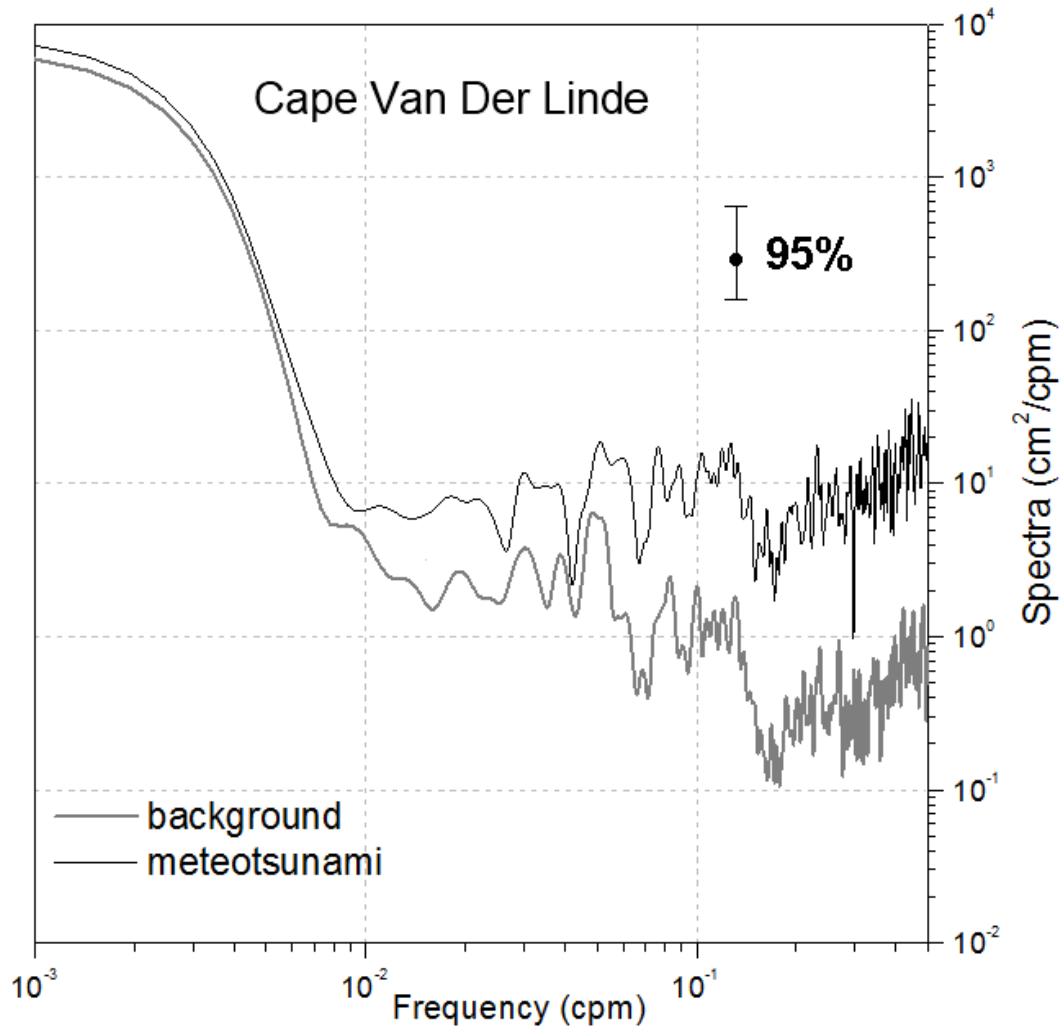

Figure 12b. Spectra of the background and of the meteorological tsunami sea level oscillations at the station of Cap Van der Linde, Urup Island.

At the Malokurilskaya Bay gauge an increase in amplitude began later than at the Cape Van der Linde. It began on January 24 at 3:40 UTC. The intense oscillations had an amplitude of about 10 cm and a period of 18-20 min.

Spectra of presumed meteorological tsunami were similar to the spectra of the Simushir tsunami as well. Considerable distinctions in the energy level between the meteorological tsunami and the background spectra were observed almost for the entire frequency band, especially in the low frequency end as opposed to that shown in Figure 12c.
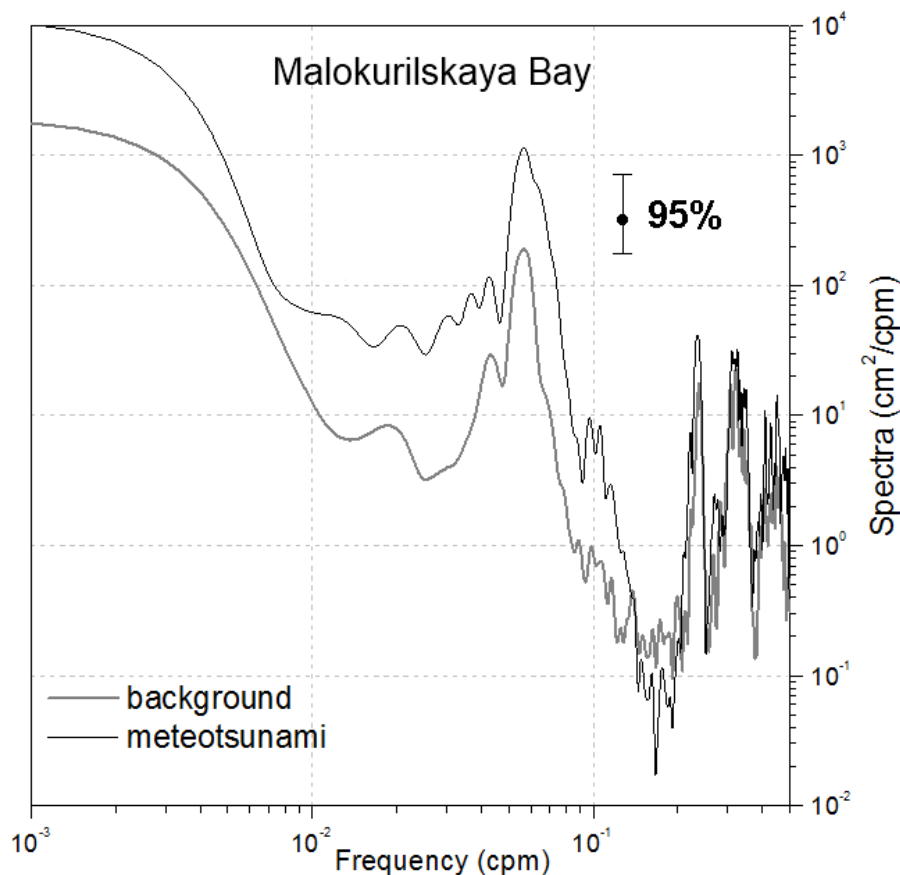
Figure 12c. Spectra of background and meteotsunami caused sea level oscillations in the Malokurilskaya Bay, Shikotan Island.

5. CONCLUSIONS

Joint recordings of well-expressed groups of waves at Hanasaki (on the oceanic coast of Hokkaido Island) and at Malokurilskaya Bay (Shikotan Island) and their considerable delay in comparison with the estimated times of arrival is a main characteristic feature of the Indonesian tsunami of January 4, 2009. The time discrepancy can be attributed to the effect of tsunami energy trapping by the shelf of Japan. The closeness of the wave group period on a shelf of Japan with resonant period of the Malokurilskaya Bay was clear evidence of the Indonesian tsunami recording in spite of the great distance from the source. Edge waves did not reach the gauges near the Iturup and Urup Islands, so the Indonesian tsunami could not be identified there.

The Simushir tsunami of 15 January was clearly recorded by the bottom pressure gauge in the Malokurilskaya Bay. A well-expressed group of waves was identified with the period of the main resonant mode occurring about four hours after the first wave arrival. The same delay was observed in the case of the Simushir tsunami on 15 November 2006. This delay was attributed to tsunami energy trapping by the shelf (Rabinovich et al, 2008). More than likely this same effect also caused the delay of the Simushir tsunami arrival on January 15, 2009.

We could not determine the tsunami arrival time and tsunami heights at the Kitoviy bay and Van der Linde gauges due to very high noise levels. This noise was caused by severe storm which was generated by deep cyclone in the southern part of the Sea of Okhotsk. To estimate the characteristics of the tsunami we were forced to use averaging with a 3-minute time window. The tsunami arrival time was 18:49 UTC at Van der Linde gauge, a one hour after of the earthquake. The maximal wave heights (8-10 cm) were observed much later, on Jan.16 from 15:43 to 16:49. Totally, the duration of oscillation was about 32 hours, which is very long for the relatively weak tsunami.

We did not determine a tsunami arrival time at Kitoviy Bay station. The intensity of sea level oscillations has steadily increased from 15:00 on Jan.15 to 5:00 on Jan. 16, when a maximum height of about 97 cm was recorded. The high amplitude sea level fluctuations continued long enough, until 12:40. The high intense oscillations also were recorded at 15:50, about at the same time, when the maximal waves were recorded at the Cape Van der Linde gauge.

The significant increase in energy was found in the both high- and low-frequency bands of the spectrum (at the periods 30-60 min and less than 5 min). The energy increasing in the high-frequency band was caused by strong storm. The weaker increase in energy fluctuations at low frequencies was observed at other stations too.

The anomalous sea level oscillations were recorded by all stations on January 23-24, 2009. We did not find any strong earthquakes in the area of Pacific Ocean in this day in the NEIC seismological catalogue. Most probably, this event was caused by meteorological forces (so-called "meteorological tsunami"). These oscillations were similar to Simushir tsunami-caused oscillation, the considerable distinctions in the energy level between meteotsunami and background spectra is observed almost for the entire frequency band.

The examples of Simushir tsunami on January 15 and meteotsunami on January 23-24, 2009 illustrate the difficulty of tsunami signal determination against the noise. The obtained results are important for the Sakhalin Tsunami Warning Service which has mostly shallow-water real-time tsunami recorders.

ACNOWLEDGMENTS

REFERENCES

Djumagaliev, V.A, Rabinovich, A.B. and Fine, I.V (1994). Theoretical and experimental estimation of transfer peculiarities of the Malokurilsk Bay coast, the Island of Shikotan, *Atmosph. Oceanic Physics*, 30 (5), 680-686,

Dykhan B.D., Zhak V.M., Kulikov E.A. et al. (1981).The first in the world tsunami registration in the deep ocean, *Dolady USSR Academy of Sciences, Earth science. Section*, 257 (5), 1088-1092. (in Russian, English translation).

Kabatchenko I.M., Kosyan R.D., Krasitsky V.P., Serykh V.Ya., Shehvatov B.V. Field experience of the wave recorder – tide gauge VM-04, *Journal Oceanology,* 47, (1), 150-155. (in Russian, English translation)

Levin B.V., Chernov A.G., Shevchenko G.V., Kovalev P.D., Kovalev D.P., Kurkin A.A., Likhacheva O.N., Shishkin A.A. (2009). The first results of long wave registration in the range of tsunami periods in the region of Kuril Ridge on a distributed station network, *Doklady Earth Sciences*, 425 (5), 874-879.

Lobkovsky L. I., Rabinovich A. B., Kulikov E. A., Ivashchenko A. I., Fine I. V., Thomson R. E., Ivelskaya T. N. and Bogdanov G. S. (2009) Kuril Earthquakes and Tsunamis of 15 December 2006 and 13 January 2007: Observations, analysis and numerical modeling, *Journal Oceanology, 49* (2), 166-181. (in Russian, English translation)

Rabinovich A.B., Lobkovsky L.I., Fine I.V., Thomson R.E., Ivelskaya T.N. and Kulikov E.A. (2008) Near-surface observations and modeling of the Kuril Islands tsunamis of 15 November 2006 and 13 January 2007, *Advances in Geosciences*, Vol. 14, pp.105-116.

Zhak V.N., Soloviev S.L. (1971). Distant registration of tsunami type weak waves on the shelf of Kuril Islands, *Dolady USSR Academy of Sciences, Earth science. Section*, 198 (4), 816-817. (in Russian, English translation).
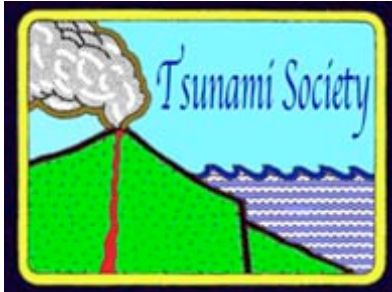
LOCAL SITE CONDITIONS INFLUENCING EARTHQUAKE INTENSITIES AND SECONDARY COLLATERAL IMPACTS IN THE SEA OF MARMARA REGION - Application of Standardized Remote Sensing and GIS-Methods in Detecting Potentially Vulnerable Areas to Earthquakes, Tsunamis and Other Hazards

George Pararas-Carayannis[1], Barbara Theilen-Willige[2], Helmut Wenzel[3]

[1]Tsunami Society International, Honolulu, Hawaii, USA
[2]Technical University of Berlin, Institut für Angewandte Geowissenschaften, GERMANY
[3]VCE Holding GmbH, Wien, AUSTRIA

ABSTRACT

    The destructive earthquake that struck near the Gulf of Izmit along the North Anatolian fault in Northwest Turkey on August 17, 1999, not only generated a local tsunami that was destructive at Golcuk and other coastal cities in the eastern portion of the enclosed Sea of Marmara, but was also responsible for extensive damage from collateral hazards such as subsidence, landslides, ground liquefaction, soil amplifications, compaction and underwater slumping of unconsolidated sediments. This disaster brought attention in the need to identify in this highly populated region, local conditions that enhance earthquake intensities, tsunami run-up and other collateral disaster impacts. The focus of the present study is to illustrate briefly how standardized remote sensing techniques and GIS-methods can help detect areas that are potentially vulnerable, so that disaster mitigation strategies can be implemented more effectively. Apparently, local site conditions exacerbate earthquake intensities and collateral disaster destruction in the Marmara Sea region. However, using remote sensing data, the causal factors can be determined systematically. With proper evaluation of satellite imageries and digital topographic data, specific geomorphologic/topographic settings that enhance disaster impacts can be identified. With a systematic GIS approach - based on Digital Elevation Model (DEM) data - geomorphometric parameters that influence the local site conditions can be determined. Digital

elevation data, such as SRTM (Shuttle Radar Topography Mission, with 90m spatial resolution) and ASTER-data with 30m resolution, interpolated up to 15 m) is readily available. Areas with the steepest slopes can be identified from slope gradient maps. Areas with highest curvatures susceptible to landslides can be identified from curvature maps. Coastal areas below the 10 m elevation susceptible to tsunami inundation can be clearly delineated. Height level maps can also help locate topographic depressions, filled with recently formed sediments, which are often linked with higher groundwater tables. Such areas are particularly susceptible to higher earthquake intensities and damage. The sum of risk GIS factors increases the susceptibility of local soils in amplifying seismic ground motions. Areas most susceptible to higher earthquake impacts can be identified using a systematic GIS approach, the weighted–overlay-method implemented in ArcGIS. Finally, the data obtained by remote sensing can be converted into Google Earth-kml-format and become available at no cost, to raise public disaster awareness and preparedness in the Sea of Marmara region.

Keywords: Sea of Marmara, Bosporus, Dardanelles, 1999 Izmit earthquake, tsunami, landslides, remote sensing, GIS methods, Digital Elevation Model, Shuttle Radar Topography.

1. INTRODUCTION

On August 17, 1999, a large destructive earthquake (named as the "Kocaeli earthquake") struck northwest Turkey and generated a destructive tsunami within the enclosed Sea of Marmara. This was the strongest earthquake to strike Northern Turkey since 1967. Its epicenter was near the Gulf of Izmit, a densely populated area. Official estimates indicated that about 17,000 people lost their lives and thousands more were injured. Most of the destruction and deaths resulted from secondary collateral impacts at locations along coastal area of the Sea of Marmara that were particularly vulnerable because local geologic site conditions exacerbated earthquake intensities. Following the disaster it was determined that there was a need to identify and map such vulnerable sites.

The present study provides a background of the disaster, the geologic setting that makes this region vulnerable and an analysis of how standardized remote sensing techniques, satellite imageries, digital topographic data and a systematic GIS approach that is based on Digital Elevation Model (DEM) data, can be integrated to help determine geomorphologic/topographic settings and identify specific geomorphometric parameters that influence local site conditions which enhance secondary, collateral, disaster impacts.

2. THE IZMIT EARTHQUAKE OF AUGUST 17, 1999

Many seismic stations around the world measured the earthquake. Its origin time was 00:01:39.80 (UTC), 03:01:37 am (local time) and its focal depth was shallow (17 km)(USGS). The epicenter was at 40.702 N, 29.987 E (USGS), near the town of Gölcük on the western segment of the North Anatolian Fault. There were small differences in magnitude determinations. The surface wave magnitude was given as 7.8 (USGS). The Moment Magnitude was given as Mw=7.4 (USGS; Kandilli). The Duration Magnitude was given as 6.7 (Kandilli) and the Body Wave Magnitude at 6.3

(USGS) and 6.8 (British Geological Survey), respectively. The earthquake resulted from right-lateral strike-slip movement on the fault. Numerous aftershocks with magnitude above 4 were recorded after the main earthquake. The first of the aftershocks (magnitude of 4.6) occurred 20 minutes later. Several others followed in subsequent days. According to the USGS and Kandilli most of the aftershock activity was confined to the region bounded by 40.5-40.8N and 29.8-30.0E, which covers the area between Izmit and Adapazari to the east of the epicenter (Pararas-Carayannis, 1999). However there was a cluster of aftershocks near Akyazi and Izmit.

On 31 August, a strong aftershock killed one person, injured about 166 others and knocked down some of the buildings that were already weakened by the main quake. Surprisingly the aftershocks caused a great deal of damage, which indicated that local conditions, exacerbated earthquake intensities of even weaker events to have secondary collateral impacts.
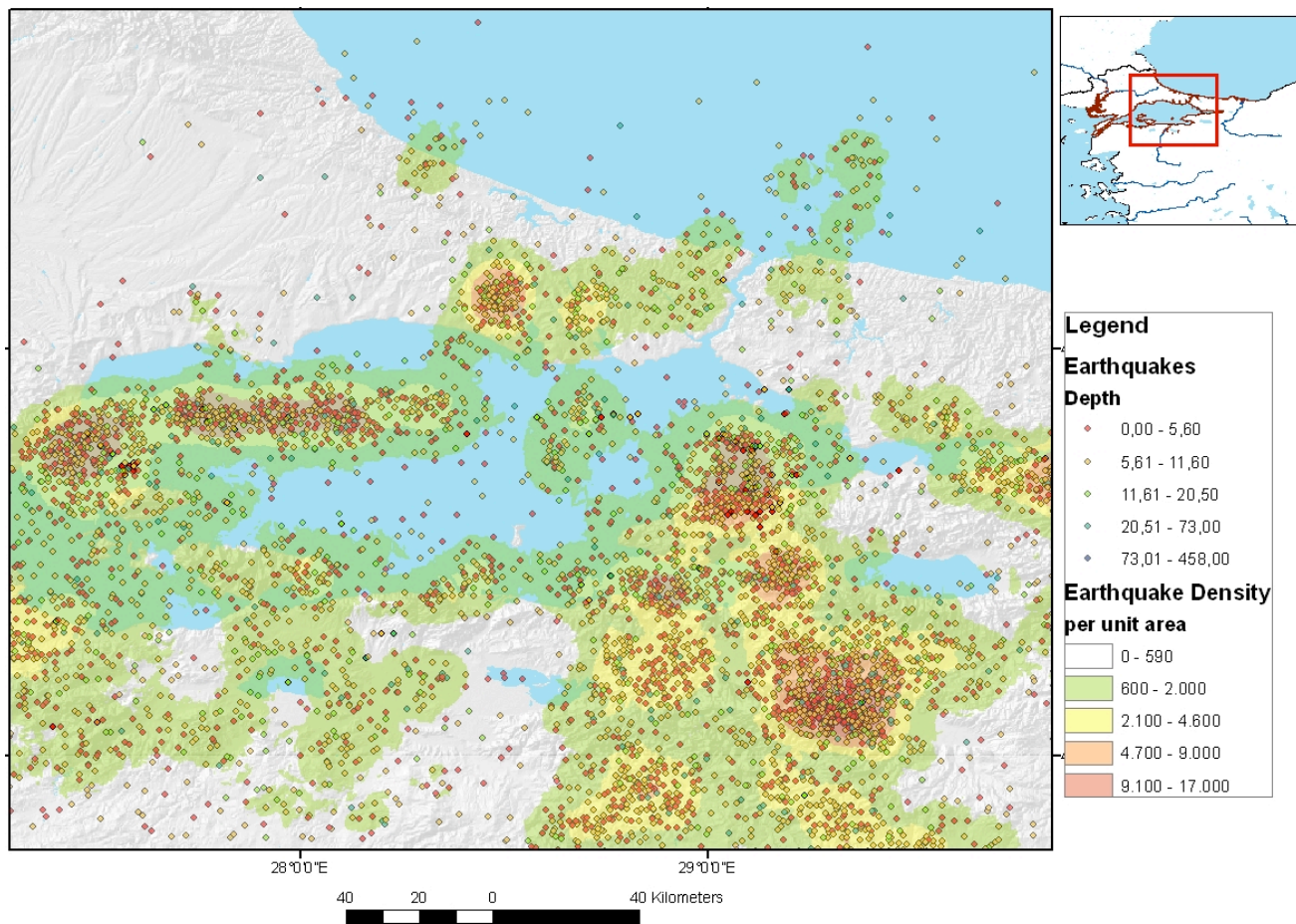

Fig. 1. Earthquake density in Sea of Marmara Region, Earthquake data: ISC, Bogazici University, Kandilli Observatory & Earthquake Research Institute, World Stress Data.
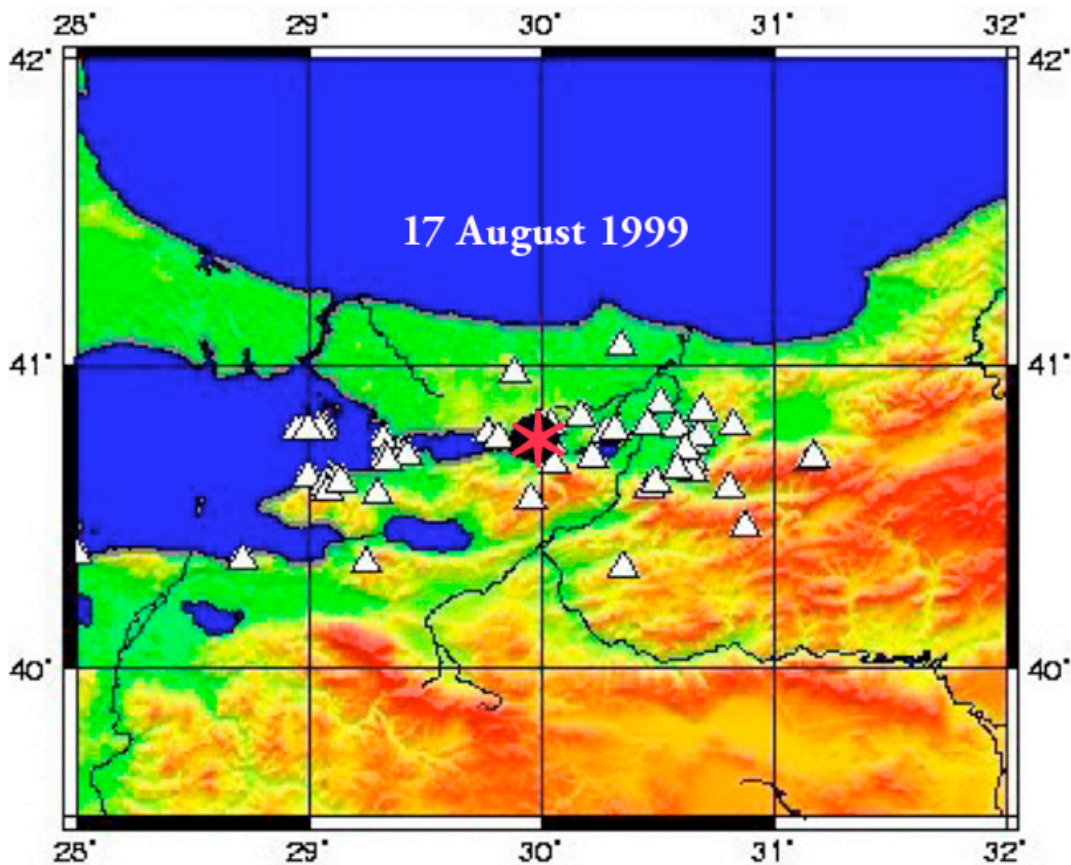
Figure 2. Epicenter and distribution of large aftershocks of the 17 August 1999 earthquake (modified after KOERPI*)*

3. THE TSUNAMI OF AUGUST 17, 1999 IN THE SEA OF MARMARA

Although the earthquake involved primarily horizontal ground displacements, slumping and landslides triggered tsunami waves which were particularly damaging in the Gulf of Izmit, perhaps because of convergence and a funneling effect. The long duration of the earthquake's ground motions (45 seconds), the directivity of the surface seismic waves, the proximity of the epicenter to the Sea of Marmara and the Gulf of Izmit, and the overall orientation of the affected area, strongly support that the tsunami was generated in the Gulf of Izmit, in the eastern portion of the Sea of Marmara. The tsunami waves had an extremely short period of less than a minute, which also supports the premise that the source was the localized subsidence of coastal areas and the underwater slumping of unconsolidated sediments, rather than larger scale tectonic movements which involved primarily lateral motions (Pararas-Carayannis, 1999). An initial recession of the water was observed at both

sides of Izmit Bay immediately after the quake, followed by tsunami waves which had an average run-up of 2.5 m. along the coast. Maximum run-up was 4 m in Golcuk where there was considerable damage to the naval base facilities. In fact, Golcuk and several coastal areas are now flooded permanently as a result of tectonic subsidence and landslides. Also, large coastal portions of the town of Degirmendere remained flooded as a result of subsidence - with sea level reaching the second floors of apartment buildings. Similar permanent flooding, but to a lesser extent, occurred also at Karamursel.
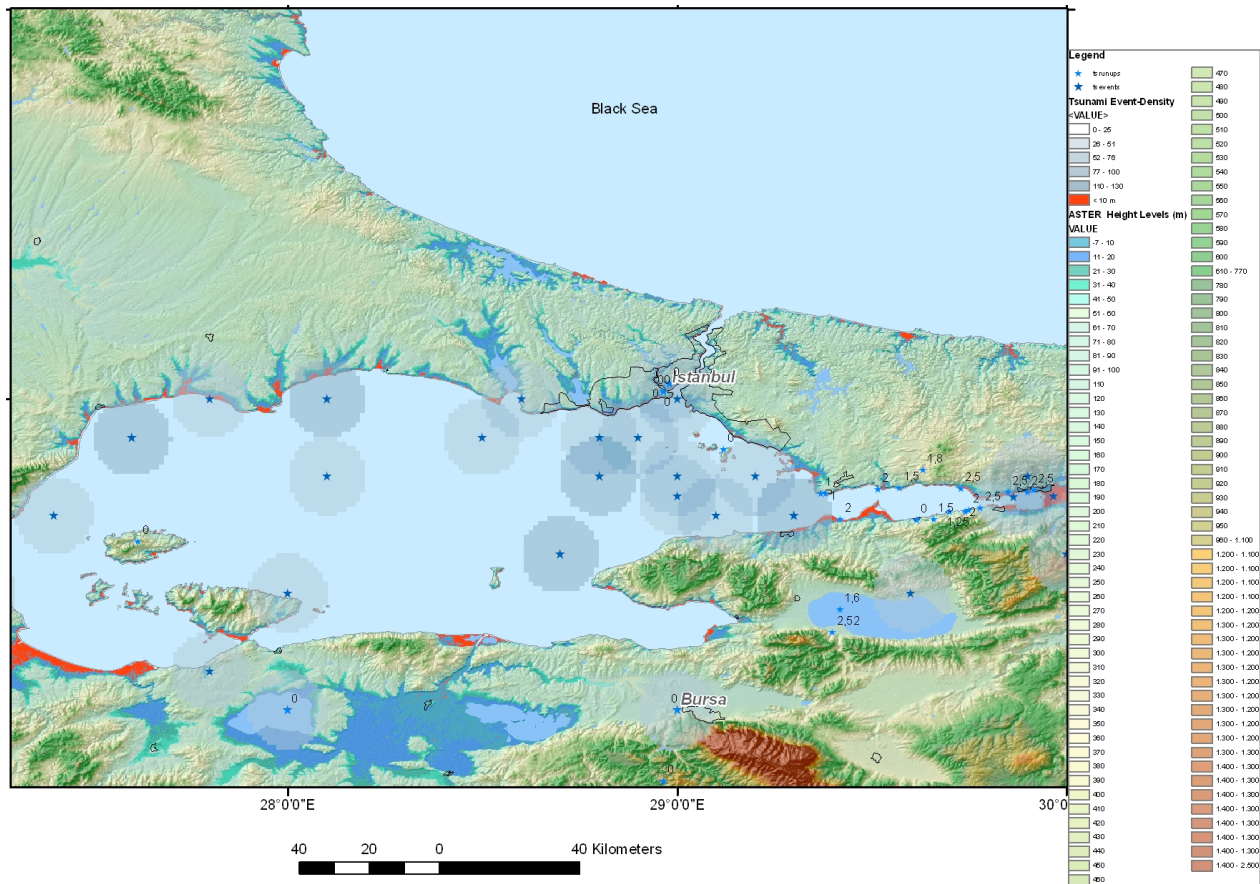

Figure 3: Overview of tsunami events and run-up heights according to NASA tsunami catalogue. The red areas indicate heights below 5 m.

The westward propagation of the seismic ruptures along the North Anatolian Fault (NAF) during the 20th century has increased the probability that the next rupture will be located offshore, in the Marmara Sea, in the prolongation of the 1999 Izmit earthquake faulting. Also, there is a high probability that a destructive tsunami will be generated. Historical records indicate that that more than 90 tsunamis have occurred along the Turkish coasts between 1410±100 BC and 1999 AD. Near Izmit Bay, tsunamis occurred in: 325; 24 August 358; 8 November 447; 26 September 488; 15 September

553; 15-16 August 555; 14 December 557; 715; 740; 19 April 1878; 10 May 1878; and 18 September 1963 (Altinok et. al., 1999). Strong earthquakes in the Marmara Sea in 1509, and in May 1766, broke submarine parts of the NAF, in the vicinity of Istanbul and generated tsunamis. Future tsunamis may be triggered either by submarine co seismic displacements or by landsliding (Hebert, 2005).

The lesson learned from this event is that tsunamis can occur in any body of water since a variety of mechanisms can generate them. Even earthquakes involving primarily horizontal ground motions (strike-slip type of faulting) can generate tsunamis by triggering slope failures and underwater landslides. Obviously the susceptibility of coastal regions along the Sea of Marmara needs to be carefully evaluated.

Figure 4: Extreme destruction from collateral ground liquefaction and subsidence (source:)

4. SEISMOTECTONIC AND GEOLOGIC SETTING

Before discussing how standardized remote sensing and GIS methods can be applied in the identification of sites potentially vulnerable to earthquakes, tsunamis and other collateral hazards, we must first review briefly the seismotectonic and geologic setting of this region.

The Sea of Marmara is an inland sea separating Asia Minor from Europe. It is 280 km (175 miles) long and almost 80 km (50 miles) wide at its greatest width. On its northeast end, it connects with the Black Sea through the Bosporus Strait. On its southwest end it connects with the Aegean Sea through the Dardanelles. Although its total area is only 11,350 square km (4,382 square miles), its average depth is about 494 m (1,620 feet), reaching a maximum of 1,355 m (4,446 feet) in the center.

The sea was formed as a result of tectonic movements that occurred about 2.5 million years ago, in the Late Pliocene (Pararas-Carayannis, 1999).

The excessive seismicity of this particular region can be explained by current geophysical knowledge of its structural development. Turkey is being squeezed sideways to the west as the Arabian plate pushes into the Eurasian plate. The north Anatolian fault forms the edge of this Turkish (Anatolian) crustal block so that destructive earthquakes happen regularly along it as different sections break (Pararas-Carayannis, 1999).

The earthquake of August 17, 1999 occurred along the long, east-west trending, great North Anatolian Fault Zone (NAFZ) - known to be the most prominent active fault system in Northwestern Turkey. The NAFZ is a major fracture that traverses the Northern part of Asia Minor and marks the boundary between the Anatolian tectonic plate and the larger Eurasian continental block. It has been the source of numerous large earthquakes throughout history. The NAFZ splits into three strands at the eastern part of the Marmara Sea. The northern strand passes through Izmit Bay, traverses Marmara Sea and reaches to the Saros Gulf (Barka and Kadinsky-Cade, 1988). The central fault zone passes through Izmit Bay, traverses the Sea of Marmara and reaches the Saros Gulf to the southeast. This great fault system has many similarities to the San Andreas fault system in California. Earthquakes involve primarily horizontal ground motions (strike-slip type of faulting). Because of this unstable tectonic system, the area is considered as one of the most seismically active zones of the world. In the last hundred years, numerous large earthquakes have also occurred along the NAF, in the western part of the country. Beginning with an earthquake in 1939, several more quakes - with Richter magnitudes greater than 6.7 - struck in progression along adjacent segments of the great fault (Pararas-Carayannis, 1999). The August 17, 1999 Izmit earthquake was the eleventh of such a series that have broken segments of the NAF, in both eastward and westward direction. Fig. 5 shows the epicenter of the earthquake near Izmit, as well as the location and sequence of previous events. The sequence of historic events indicates that the next destructive tsunamigenic earthquake could occur west of the 1999 event, in the Sea of Marmara.
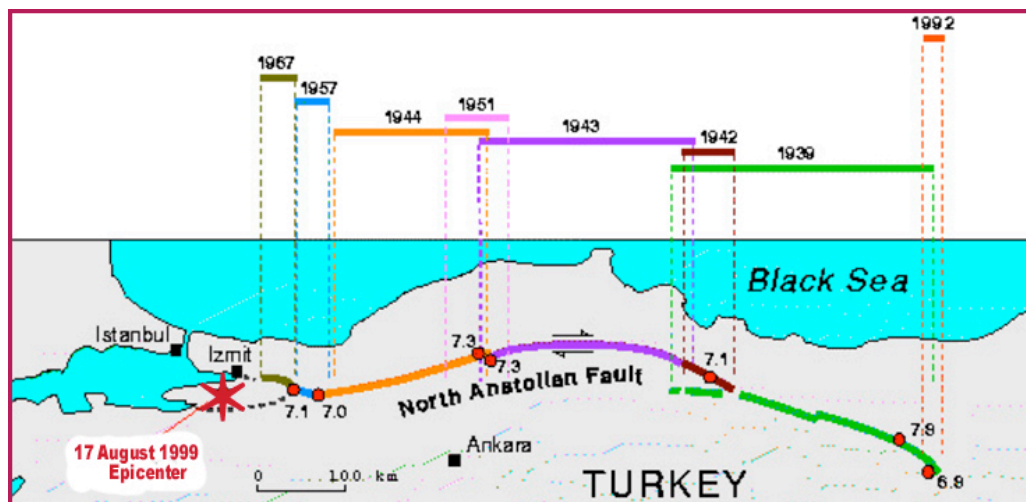

Figure 5: Historical Earthquake Activity Along the Northern Anatolian Fault (modified after Kandilli)

5.1 Earthquake's Surface Rupture and Ground Displacements

The earthquake's surface rupture extended for about 100 km east of Golcuk, but did not continue southeast and did not join the rupture of the 1967 earthquake - the last event in this region. Instead, the rupture turned northeast near Akyazi, where a cluster of aftershocks subsequently occurred. Ground displacements of about 1.5 m were measured in this area. Subsequent field studies indicated right lateral ground displacements ranging from 2.5-3 m up to 4 m, with a maximum of 4.2 m east of Lake Sapanca. Ground displacements between Lake Sapanca and the Gulf of Izmit were about 2.60 m. Additionally, there was evidence of about 2 meters subsidence along the north side of the fault's block - which was particularly evident along the coastline at Golcuk, where tsunami waves and major flooding occurred (Pararas-Carayannis, 1999). Such tectonic ground displacements are characteristic of major earthquakes along the NAF and have been responsible for the development of local geologic conditions, which exacerbate earthquake intensities and the potential impact of collateral hazards in the Sea of Marmara region.
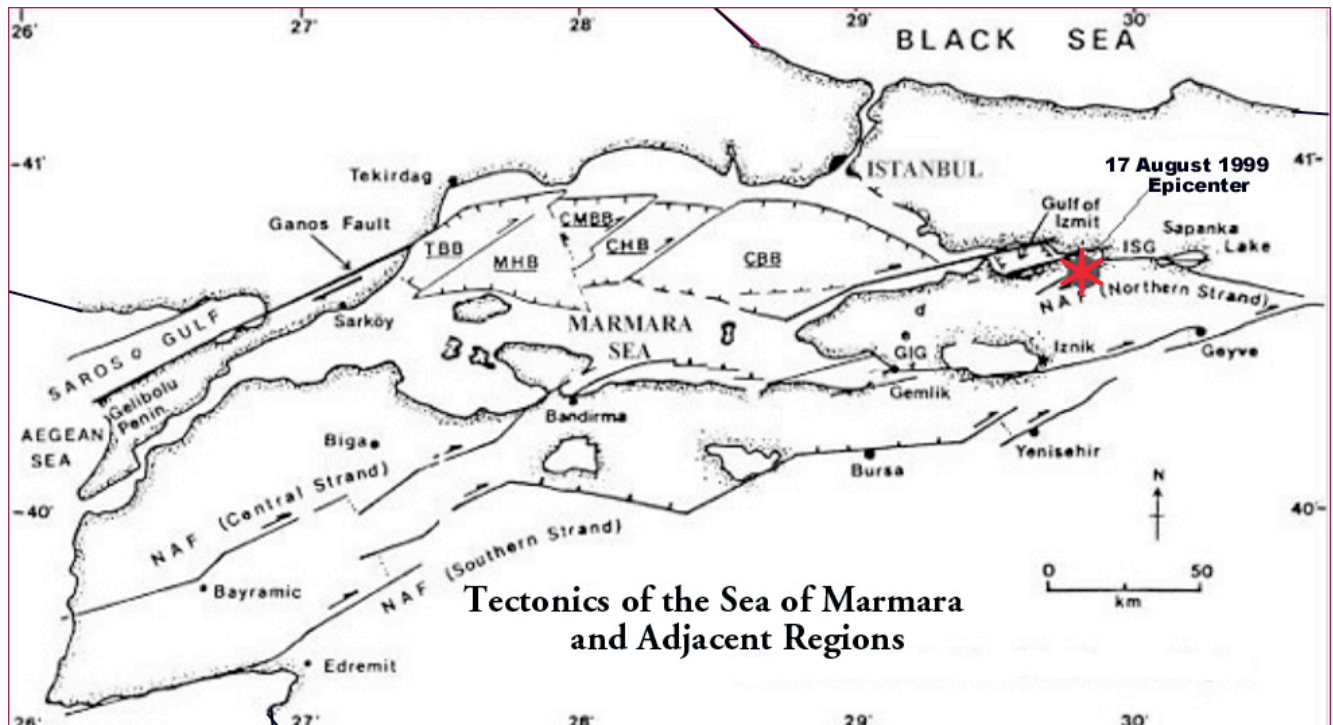

Fig. 6: Tectonic Map of the Marmara Region and location of the earthquake (source:).

6. POTENTIAL COLLATERAL HAZARDS ASSOCIATED WITH EARTHQUAKES AND TSUNAMIS IN THE SEA OF MARMARA REGION

The entire Sea of Marmara is traversed by numerous deformed and offset branches and strands of the NAF, where destructive tsunamigenic earthquakes can occur. The 1999 earthquake occurred near the Gulf of Izmit along an offset central branch of the NAF. The E-W trending Izmit Bay is a tectonically active basin which is particularly susceptible to earthquakes, tsunamis and collateral hazards such as subsidence, landslides, ground liquefaction, soil amplifications, compaction and underwater slumping of unconsolidated sediments. The entire bay area is covered mainly by fine-grained sediments from fluvial and littoral processes. When the 1999 earthquake struck, the local geologic site conditions exacerbated earthquake intensities.

During the first two days following this earthquake and tsunami, the severity of destruction and the losses of human lives in the region were grossly underestimated because of problems with access and communications. Almost the entire infrastructure of the region and all industrial facilities located along the coastal area of Izmit Bay were severely damaged. There was great destruction within 20 km of Gölcük that ranged from small displacements to complete collapses of coastal structures such as ports, jetties, cranes and piping systems. The navy base and shipbuilding yard at Gölcük were considerably damaged and at least 400 sailors and high ranking officers were killed. Rescue operations were delayed because of heavy damage on the major highway connecting Istanbul to Ankara and alternate roads were blocked. Many apartment blocks collapsed completely, causing the death of thousands of people. A fire at the Tupras oil refineries, which refine almost 90% of Turkey's oil, threatened to take over other industrial sites and took five and a half days to contain and extinguish (ERDIK, 2000). Also, subsidence, coastal landslides and tsunami waves caused destruction at Degirmendere and Karamursel.

If an earthquake and tsunami disaster similar to the 1999 or 1509 were to strike again the Sea of Marmara region, closer to metropolitan Istanbul, thousands of people could lose their lives and the destruction to infrastructure facilities and cultural sites would be severe. It would take many years to recover from the economic damage and to repair the infrastructure. There could be major damage to trains and stations. The Strait of Bosporus is of great economic importance. Five times the amount of ships pass through it than the Panama Canal every year. Two million people commute across it every day. Another severe earthquake could seriously damage the three major bridges and tunnel across the Golden Horn. Also, since they are sections of the Bosporus that are only 700 meters wide an earthquake-induced landslide or a collateral hazard could render it non-navigable.

Because of the economic consequences, such potential collateral disaster scenarios cannot be overlooked. When the Treaty of Montreux was signed in 1936 (to provide unrestricted passage of the Bosporus in time of peace), an average of 17 ships crossed each day the Bosporus, usually carrying grain and weighing about 13 tons. Presently, about 100-110 ships weighing as much as 200,000 tons, often carrying oil, gas, chemicals, nuclear waste, and other hazardous materials, pass through the strait each day. The question therefore arises as to what would happen if an oil tanker was sunk by a

tsunami in the Bosporus? Even a minor disaster unrelated to an earthquake could have severe economic consequences for the region. There have been at least ten major oil spills in recent times on the waterway. On 15 November 1979 the Greek ship "Eviriali" collided with the Romanian ship "Independenta", killing 43 people and releasing 94,600 tons of crude oil into the strait, with fires which burned for almost a month. Twenty-two days after this collision and a failed containment attempt by the Turkish Navy, the "Independenta" exploded, dumping 380 barrels of oil to the port of Hydarpasa. More recently, in March of 1994, the Cyprian oil tanker "Nassia", carrying 19 million gallons of crude oil from the Russian port of Novorssyisk, collided with an empty cargo ship at the entrance of the Bosporus, resulting in 30 deaths. Three of its ten tanks ruptured, the ship drifted unguided and burned for more than a hundred hours. The accident resulted in $1 billion in damages, and forced the closing of the waterway for a week. Certainly an earthquake or a tsunami could cause greater economic disasters from collateral impacts in the narrow strait.

Similar hazard vulnerability can be expected on the other side of the Sea of Marmara. The Dardanelles strait, or Hellespont, connecting with the Northern Aegean Sea, is 61 kilometers long but only 1.2 to 6 kilometers wide, with depth averaging 55 meters deep (maximum depth of 82 meters). A major branch of the North Anatolian Fault Zone, the Ganos Fault traverses the Gallipoli Peninsula along the Gulf of Saros. A large-scale landslide induced by an earthquake, or the sinking of a large ship, could render this important waterway non-navigable. Losing either of the straits on opposites sides of the Sea of Marmara would have considerable economic consequences, not only for Turkey, but for Russia, Central Asia and Europe. Thus, it becomes obvious that a program of disaster preparedness for the entire region requires proper identification of specific site vulnerabilities to natural disasters and to the potential impact of collateral hazards.

7. APPLICATION OF STANDARDIZED REMOTE SENSING AND GIS-METHODS IN DETECTING POTENTIALLY VULNERABLE AREAS TO EARTHQUAKES, TSUNAMIS AND OTHER HAZARDS IN THE SEA OF MARMARA REGION.

As the 1999 disaster demonstrated, local site conditions exacerbate earthquake intensities and can result in collateral destruction. Generative causes may include a combination of tectonic movements associated with an earthquake or major sub aerial or underwater slides which can generate destructive local tsunamis. Secondary phenomena associated with a large earthquake will depend on the energy release, the physical rupture along the fault, the propagation path of surface seismic waves and the magnitude and duration of the dynamic, near-field, strong motions. Earthquake ground motions of high intensity could result in strong accelerations or ground liquefaction (Pararas-Carayannis, 1999) which can also trigger landslides, sudden subsidences, slumping or the generation of destructive waves.

However, a systematic GIS approach based on SRTM data (Shuttle Radar Topography Mission, with 90m spatial resolution) and ASTER-data (with 30m resolution, interpolated up to 15 m), or data from the Digital Elevation Model (DEM), can help extract geomorphometric factors and thus identify sites that are potentially vulnerable in the Sea of Marmara region. For a geomorphologic

overview and for deriving the characteristic, geomorphologic features of vulnerable sites, terrain parameters and morphometric maps can be extracted from SRTM and ASTER DEM data, such as shaded relief, aspect and slope degree, minimum and maximum curvature, or profile convexity maps, using ENVI / CREASO and ArcGIS / ESRI software. Such methods can help identify sites with steep slope gradients, sites characterized by flat depressions, or sites covered by unconsolidated sediments.

With the use of remote sensing data, the causal factors can be determined systematically. With proper evaluation of satellite imageries and of digital topographic data, specific geomorphologic/topographic settings that enhance disaster impacts, can be identified. Areas with the steepest slopes can be identified from slope gradient maps. Areas with highest curvatures susceptible to landslides can be identified from curvature maps. Factors such as height levels, slope gradients, terrain curvature and traces of faults are combined with lithologic and seismotectonic information in a GIS database. Of course, many other factors play an important role and, if available, should be included in the database. The approach presented here is meant to serve as a first basic data stock in getting a perception of potential sites susceptible to higher earthquake shock and for the planning of additional geotechnical investigations.

LANDSAT ETM and DEM data can also be used as layers in generating a Hazard GIS database for the Sea of Marmara region. To enhance the LANDSAT ETM data, digital image processing procedures can be carried out. With digital image processing techniques, maps can be generated to meet specific requirements and for risk site mapping. As a complementary tool, Google Earth Pro Software can be used in order to benefit from the high-resolution 3D imageries of the coastal areas (http://earth.google.com/).

Coastal areas below the 10 m elevation susceptible to tsunami inundation can be clearly delineated from hypsographic maps. The same maps can help locate topographic depressions that may be filled with alluvial deposits, which are often linked with higher groundwater tables. Such areas are particularly susceptible to higher earthquake shock and damage. The sum of risk factors characterizes the susceptibility of local soils in amplifying seismic ground motions. Areas most susceptible to higher earthquake impacts can be identified using a systematic ArcGIS approach, map software and the weighted–overlay-method. Finally, the data obtained by remote sensing can be converted into Google Earth-kml-format and become available at no cost, to raise public disaster awareness in the Sea of Marmara region.

The present study provides only a few examples of the methodology that could be adopted to generate maps that can illustrate susceptible sites to secondarily induced, collateral hazards in the region. Figure 7 illustrates the systematic GIS-Aproach that can be used in developing earthquake susceptibility maps. Figure 8 indicates the causal factors that influence earthquake ground intensities, particularly for sites that have unconsolidated sedimentary covers or steep slope gradients and how these factors can be extracted, based on SRTM and ASTER data, geologic maps and evaluations of LANDSAT data. Finally, Figure 9 illustrates areas of the Eastern Sea of Marmara that are susceptible to higher earthquake shock according to morphometric and geologic surface properties.
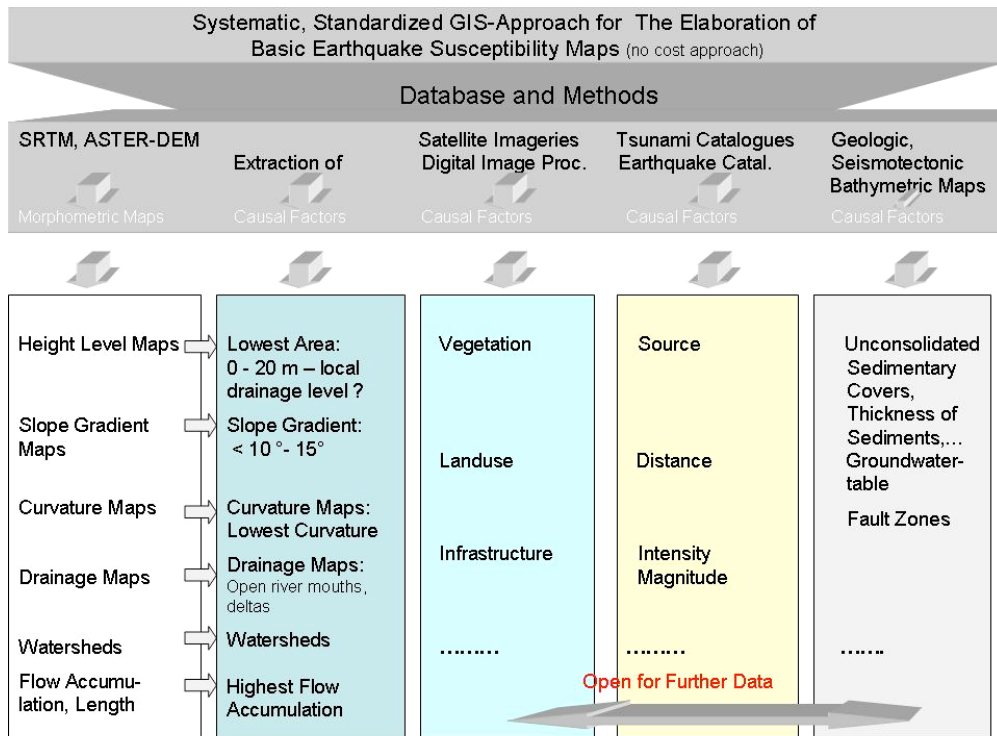
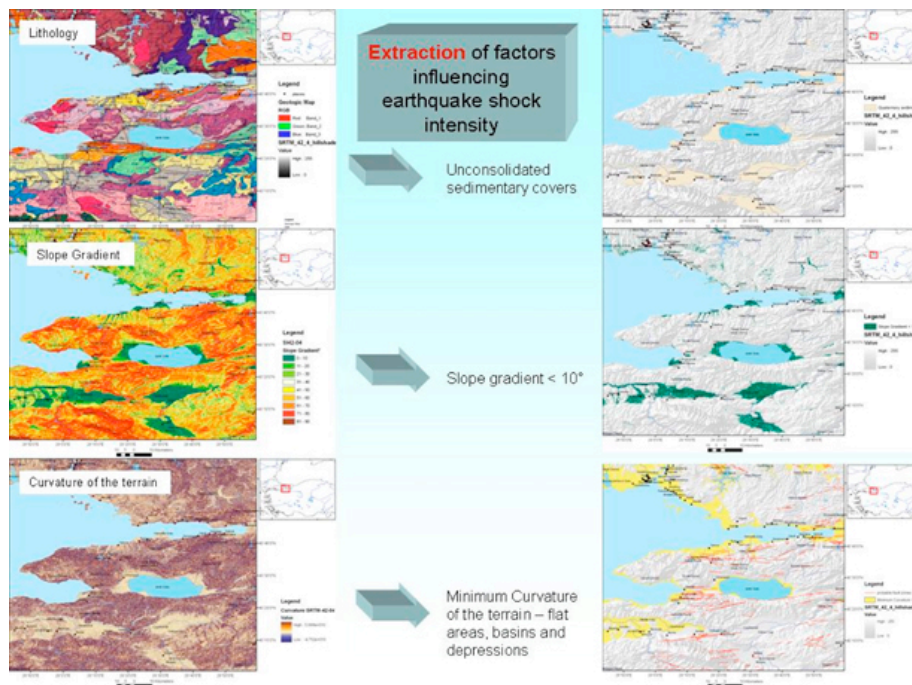Fig. 7: Basic GIS approach.

Fig.8: Extraction of some causal factors based on SRTM and ASTER data, geologic maps and evaluations of LANDSAT data.
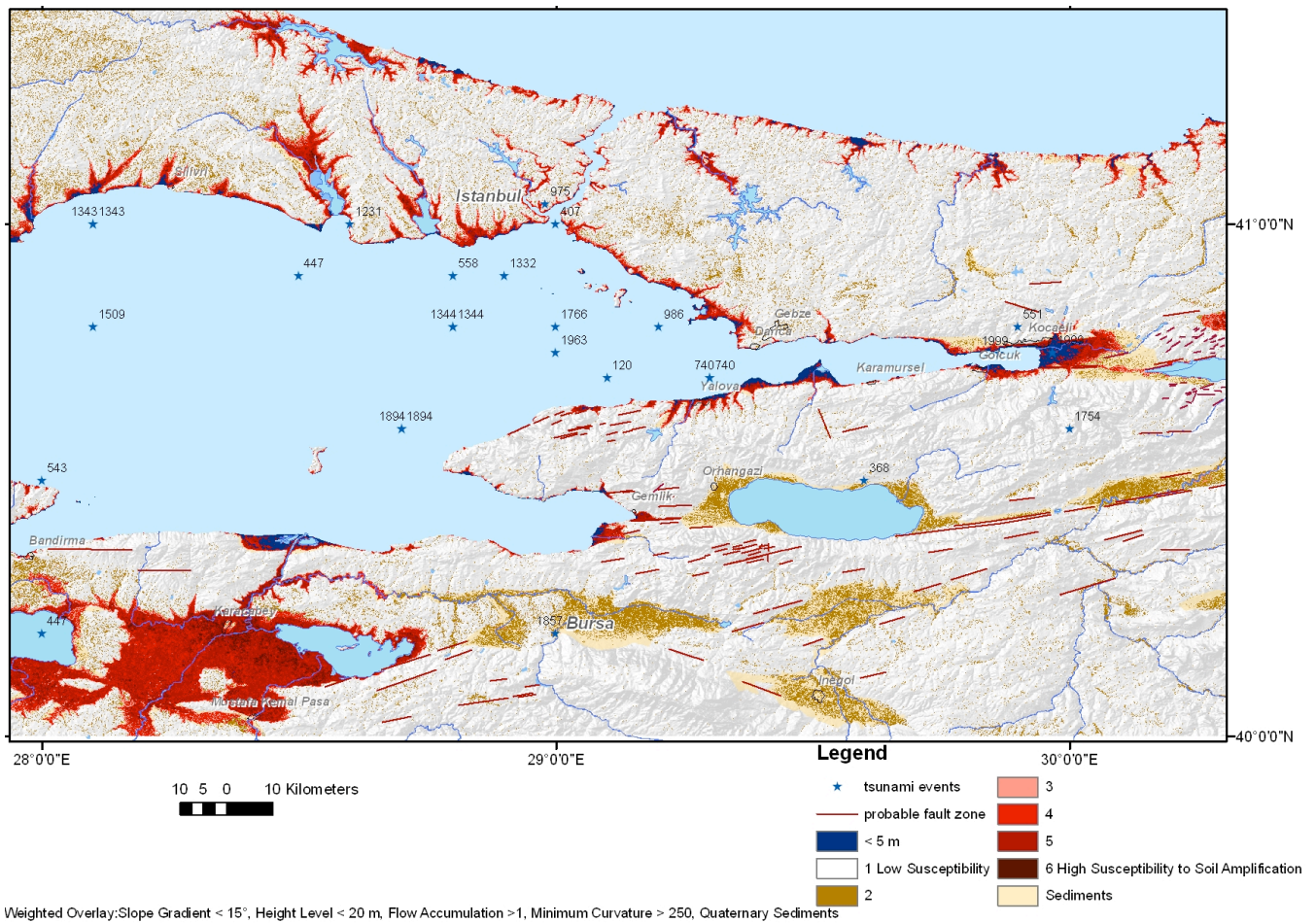
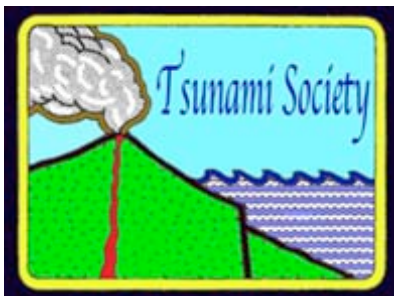Fig. 9: Areas susceptible to higher earthquake shock according to morphometric and geologic surface properties.

REFERENCES

Altinok,Y. et al.(2001): Historical tsunamis in the Sea of Marmara.- ITS,2001, Proceedings, Session 4, Number 4-2

S©ìrensen,M.B., Ivo Oprsal, Sylvette Bonnefoy-Claudet, Kuvvet Atakan , P. Martin Mai , Nelson Pulido and Caglar Yalciner (2006): Local site effects in Ataköy, Istanbul, Turkey, due to a future large earthquake in the Marmara Sea.- *Geophysical Journal International, **Volume 167 Issue 3, Pages 1413 - 1424*

Altinok, Y., Alpar, B., Ersoy, S., and A. C. Yalciner, (1999). Tsunami Generation of the Kocaeli Earthquake of August 17, 1999 in Izmit Bay; coastal observations, bathymetry and seismic data. Turkish Journal of Marine Sciences 5 (3): 131-148 (1999). http://www.drgeorgepc.com/TsunamiTurkey.html

Armijo, R., Meyer, B., Navarro, S., King, G. and Aykut Barka (2002): Asymmetric slip partitioning in the Sea of Marmara pull-apart: a clue to propagation processes of the North Anatolian Fault?- Terra Nova, Vol 14, No. 2, 80–86, 2002 Blackwell Science Ltd.

Ansal, A., M. Erdik, J. Studer, S. Springman, J. Laue, J. Buchheister, D. Giardini, D. Faeh , D. Koksal (2004). Seismic Microzonation for Earthquake Risk Mitigation in Turkey.- 13th World Conference on Earthquake Engineering, Vancouver, B.C., Canada, August 1-6, 2004, Paper No. 1428.

Barka, A.A. and Kadinsky-Cade, K. (1988). Strike-slip fault geometry in Turkey and its influence on earthquake activity, Tectonics, 7: 663-684

Erdik, M. (2000): Report on 1999 KOCAELI and DÜZCE (Turkey) Earthquakes.- Bogazici University, Dept. of Earthquake Engineering, 81220 Cengelkoy, Istanbul, Turkey

Hebert, H., Francois Schindele, Yildiz Altinok, Bedri Alpar, Cem Gazioglu (2005): Tsunami hazard in the Marmara Sea (Turkey): A numerical approach to discuss active faulting and impact on the Istanbul coastal areas.- Marine Geology 215 (2005) 23– 43

Heidbach, O., Tingay, M., Barth, A., Reinecker, J., Kurfeß, D. and Müller, B., The World Stress Map database release 2008 doi:10.1594/GFZ.WSM.Rel2008, 2008. http://dc-app3-14.gfz-potsdam.de/pub/stress_data/stress_data_frame.html

Pararas-Carayannis, G., (1999). The Earthquake and Tsunami of August 17, 1999 in the Sea of Marmara, Turkey. http://www.drgeorgepc.com/Earthquake1999Turkey.html

Spence, R. (Ed. 2007): Earthquake Disaster Scenario, Prediction and Loss Modelling for Urban Areas.- LESSLOS Report No.2007/0,7IUSS Press, Pavia 2007

Taymaz, T., Tan, O. and Yolsal, S. (2004). Active Tectonics of Turkey and Surroundings: Seismic Risk in the Marmara Sea Region, In Fujii, N., Kasahara, J., Higashihara, H., and Ogawa, K. (Eds.), The Proceedings of 1st International Workshop on Active Monitoring in the Solid Earth Geophysics (IWAM04), Extended Abstract Book: p. 110-115, Task Group for Active Monitoring, Mizunami City Culture Center, Gifu, Japan, June 30 - July 3, 2004 http://www.geop.itu.edu.tr/~taymaz/docs/Taymaz_IWAM04_S3-09.pdf

Internet sources:

1)   Southern California Earthquake Center, http://www.scec.org/phase3/overview.html
2)   International Seismological Centre, http://www.isc.ac.uk/search/custom/index.html
3)   Stress Data of the WSM, http://dc-app3-14.gfz-potsdam.de/pub/stress_data/stress_data_frame.html
4)   http://map.ngdc.noaa.gov/website/seg/hazards/viewer.htm
5)   http://www.koeri.boun.edu.tr/sismo/map/en/index.html